Transmit Waveform/Receive Filter Design for MIMO Radar With Multiple Waveform Constraints

Linlong Wu, Prabhu Babu, and Daniel P. Palomar, *Fellow, IEEE*

***Abstract*—In this paper, we consider the joint design of both transmit waveforms and receive filters for a colocated multiple-input-multiple-output (MIMO) radar with the existence of signal-dependent interference and white noise. The design problem is formulated into a maximization of the signal-to-interference-plus-noise ratio (SINR), including various constraints on the transmit waveforms. Compared with the traditional alternating semidefinite relaxation approach, a general and flexible algorithm is proposed based on the majorization-minimization method with guaranteed monotonicity, lower computational complexity per iteration and/or convergence to a B-stationary point. Many waveform constraints can be flexibly incorporated into the algorithm with only a few modifications. Furthermore, the connection between the proposed algorithm and the alternating optimization approach is revealed. Finally, the proposed algorithm is evaluated via numerical experiments in terms of SINR performance, ambiguity function, computational time, and properties of the designed waveforms. The experiment results show that the proposed algorithms are faster in terms of running time and meanwhile achieve as good SINR performance as the the existing methods.**

***Index Terms*—MIMO radar, SINR maximization, joint design, waveform constraints, majorization-minimization (MM).**

I. Introduction

UNLIKE a "conventional" radar, a multiple-input-multiple-output (MIMO) radar transmits several probing waveforms simultaneously from its transmit antennas. Returns from the target and the interferers are jointly processed by the receive antennas [1]. A MIMO radar can improve the interference rejection capability and parameter identifiability, as well as provide flexibility for transmit beam pattern design [2]. There are two kinds of MIMO radar systems: MIMO radar with widely separated antennas [3] and MIMO radar with colocated antennas [4], [5]. Recently, a cognitive approach for radar systems, which capitalizes on the information obtained from the surrounding environment or the prior knowledge stored in the platform, was proposed [6], [7].

The significance of MIMO radar and the cognitive approach has recently motivated active research into the waveform design. The radar waveform design problem can be classified roughly into three categories. The first category addresses the design problem by assuming its independence from the receive filter. Both [8] and [9] considered the design of the covariance matrix of the waveform to approximate a desired spatial transmit beampattern. Based on the desired covariance matrix, [10] proposed two algorithms to synthesize the corresponding BPSK and QPSK transmitted symbols. In [11], the authors addressed the robust design of the covaraince matrix considering the uncertainty of the steering vector. The design of a unimodular sequence with low autocorrelation sidelobes is optimized by minimizing an "almost equivalent" problem instead of the original integrated sidelobe level (ISL) problem [12] and and then the authors incorporated the spectral constraint in [13]. Later, [14] considered the ISL minimization problem directly and then [15] extended the solution to the weighted case and the ℓ_p-norm case. Further, both [16] and [17] designed the sequences by shaping the auto-correlation and the cross-correlation simultaneously. In [18], the metric used for optimization is the convex combination of the Kullback-Leibler divergences between the densities of the observations. In [19], both the mutual information (MI) and the mean-square error (MSE) were used as the design criteria and the robust case was considered in [20]. In [21], the authors arrived at a quartic problem, which considers the Doppler effect under the disturbances of signal-dependent interference and white noise.

The second category of waveform design considers the receive filter with the existence of signal-independent interference. In [22]–[24], the authors considered the radar code design in the presence of colored Gaussian disturbance, and then formulated a nonconvex quadratic problem of maximizing the signal-to-noise ratio (SNR), which was solved through semidefinite relaxation (SDR) and then rank-one randomization. In [25] and [26], the authors addressed the robust case with an unknown Doppler frequency of the target. In [27], the lower Chernoff bound and the MI were considered to optimize the space-time code under non-Gausssian target scattering. In [28] and [29], the optimization criteria were extended to a general cost function, and a min-max solution to robust design, which applies to many commonly adopted performance measures, was proposed.

The third category of waveform design also considers the receive filter but with the existence of signal-dependent

Manuscript received March 21, 2017; revised August 16, 2017 and December 7, 2017; accepted December 9, 2017. Date of publication December 25, 2017; date of current version February 7, 2018. The associate editor coordinating the review of this manuscript and approving it for publication was Prof. Marco Lops. This work was supported in part by the Hong Kong RGC 16206315 research grant and in part by the Hong Kong RGC Theme-based Research Scheme (TRS) Grant T21-602/15R. *(Corresponding author: Linlong Wu.)*

L. Wu and D. P. Palomar are with the Department of Electronic and Computer Engineering, Hong Kong University of Science and Technology, Hong Kong (e-mail: lwuag@ust.hk; palomar@ust.hk).

P. Babu is with the Centre for Applied Research in Electronics, Indian Institute of Technology Delhi, New Delhi 110016, India (e-mail: prabhubabu@care.iitd.ac.in).

Color versions of one or more of the figures in this paper are available online at http://ieeexplore.ieee.org.

Digital Object Identifier 10.1109/TSP.2017.2787115

interference. In [30], an iterative method was derived for the case of an extended target and clutter, with only the finite energy constraint considered. Similarity and constant energy constraints were considered, and two alternating maximization methods were proposed in [31]. In [32], besides the typical alternating minimization method, a constrained proximal alternating minimization technique was also proposed to deal with rank deficient correlation matrices. In [33], the authors considered both the average and worst-case performance metrics of the optimal detector (with known Doppler shift) for waveform design. Then in [34], both the transmit waveform and the receive filter were considered jointly and a max-min problem was cast to robustify the SINR. The method to solve this problem is based on a relaxed alternating maximization, followed by a synthesis stage. Different from [34], which used a single filter, a Doppler filter bank was deployed at the receiver in [35]. The joint design of the transmit waveform and receive filter was also addressed in [36]–[38].

Several waveform constraints are often incorporated into the design problem with the consideration of the hardware configuration and the application scene. The constant modulus constraint [39] is often considered due to the limitations of waveform generation hardware components, and the peak-to-average ratio (PAR) constraint [26] is more general (mathematically) than the unimodular case. In the practical sense, the PAR constraint is more relaxed. The similarity constraint [22], [23] is incorporated to force the designed waveform to be similar to the reference one with desirable properties. In order to reduce the interference caused by radar systems over the coexisting telecommunication systems, a spectrum compatibility constraint [40]–[44] is considered. All these constraints are significant in practice and widely considered in the radar field.

Note that for joint design, a popular approach is to adopt the alternating optimization scheme and then resort to semidefinite relaxation (SDR) and rank-one reconstruction. The convergence of the sequence of the objective values can be claimed as long as the monotonicity of the approach and the boundedness of the objective function hold. However, solving a rank-one constrained SDP problem at each iteration is time-consuming and has no guarantee of optimality if some heuristic technique, e.g., reconstruction by randomization, on rank-one reconstruction is used, which further results in the loss of convergence of the solution (sub-)sequence.[1] In addition, some waveform constraints are necessarily incorporated into the design problem with the consideration of hardware configuration and application scenarios. However, these constraints might raise the complexity of the corresponding algorithm. For example, in [30], closed-form solutions at each iteration can be found when only the finite energy constraint is considered. If other constraints, such as the spectrum compatibility constraint, are considered, then it is not as easy as the former case. For real-time application systems, such as radar tracking and some communication networks, these above issues require a great deal of care. Thus, a new algorithm, which is not only faster than the SDR and able to guarantee both monotonicity and convergence, but also general and flexible so that various constraints can be handled within its framework, is desired.

In this paper, we develop an algorithm for the joint design problem based on the general majorization-minimization (MM) method [46], [47] and that is capable of dealing with several practical constraints. In order to illustrate the flexibility of our algorithm, we consider four commonly required constraints on the transmit waveform and for each case, we derive a corresponding specific algorithm based on the general framework. For each algorithm, we also analyze its computational cost on a per-iteration basis. Given that many existing methods are based on the alternating optimization approach, we also illustrate the connection and the difference between the derived method and such other methods. Experiments show that our method is very efficient and flexible in dealing with various waveform constraints, and achieves faster CPU time and/or higher SINR compared with the existing methods.

The rest of this paper is organized as follows. In Section II, we introduce the system model and formulate the joint design problem of interest. In Section III, we first briefly introduce the general MM method and then derive the general algorithm within the MM framework. In Section IV, we consider four constraints on the problem: the constant modulus constraint, the similarity constraint, the PAR constraint, and the spectrum compatibility constraint. At the end of this section, we give a complete description of these algorithms and analyze their computational cost. In Section V, we interpret the alternating optimization method from the perspective of the MM framework and reveal its connection with our derived method. In Section VI, we analyze the numerical performance of the proposed algorithm for each case and compare our methods with the corresponding benchmarks. Finally, the conclusions are given in Section VII.

Notation: $\mathbb{R}^n$ and $\mathbb{C}^n$ denote the n-dimensional real and complex vector space, respectively. $\mathbb{R}_{\geq 0}$ and $\mathbb{R}_{<0}$ denote the set of non-negative real numbers and the set of negative real numbers, respectively. $\mathbb{R}^{m\times n}$ and $\mathbb{C}^{m\times n}$ denote the $m \times n$ real and complex matrix space, respectively. Boldface uppercase letters stand for matrices. Boldface lowercase letters stand for column vectors. Standard lowercase letters stand for scalars. $(\mathbf{x})^T$ and $(\mathbf{x})^*$ denote the transpose and conjugate of a complex vector $\mathbf{x}$, respectively. $\mathrm{Re}(\mathbf{x})$ and $\arg(\mathbf{x})$ denote the element-wise real part and the phase of a complex vector $\mathbf{x}$, respectively. $(\mathbf{X})^T$, $(\mathbf{X})^*$, $(\mathbf{X})^H$, $\mathrm{tr}(\mathbf{X})$, $\mathrm{vec}(\mathbf{X})$, $\lambda_{\max}(\mathbf{X})$, and $\lambda_{\min}(\mathbf{X})$ denote the transpose, complex conjugate, conjugate transpose, trace, vectorization, largest eigenvalue, and smallest eigenvalue of a matrix $\mathbf{X}$, respectively. $\mathrm{Diag}(\mathbf{x})$ stands for a diagonal matrix with its principal diagonal filled with $\mathbf{x}$. $\mathbf{I}_N$ denotes the $N \times N$ identity matrix. x_i denotes the i-th element of $\mathbf{x}$. $|\cdot|$ denotes the

[1]To avoid possible misunderstanding, the convergence of the solution (sub-)sequence is defined as $\lim_{j\to+\infty}\{\mathbf{x}^{k_j}\} = \mathbf{x}^\star$, where $\mathbf{x}^\star$ is a stationary point of the optimization problem. For the alternating optimization method, if the minimum of each block subproblem is uniquely attained. Then, every limit point of $\{\mathbf{x}^k\}$ is a stationary point [45, Proposition 2.7.1]. For the case of only two blocks, the minimizer still needs to be global but not necessarily unique. In our case, it implies that the rank-one constrained SDP subproblem should be solved optimally, e.g., the complex-valued homogeneous QCQPs with the number of the constraints less than 5. Otherwise, the convergence does not hold generally and should be analyzed ad-hoc. For interested readers, please refer to [21], [35], [37] in which the alternating approach is used and the convergence to a stationary point is proved.

modulus of a complex scalar or the element-wise modulus of a complex vector. $\|\cdot\|$ denotes the ℓ_2-norm of a vector. $\otimes$ denotes the Kronecker product. $\mathcal{D}_{\mathbf{x}} f$ and $\frac{\partial f}{\partial \mathbf{X}}$ denote the derivative of a scalar function f on the vector $\mathbf{x}$ and the matrix $\mathbf{X}$, respectively. $\mathbb{E}(\cdot)$ denotes the statistical expectation.

II. System Model and Problem Formulation

Consider a colocated MIMO radar system with N_t transmit antennas and N_r receive antennas. Each transmit antenna emits a waveform $s_m(n), m = 1, \ldots, N_t, n = 1, \ldots, N$, with N being the number of samples of each transmitted pulse. Let $\mathbf{s}(n) \in \mathbb{C}^{N_t \times 1}$ represent the n-th sample of the N_t waveforms. Suppose the target of interest is located at the range-angle position (r_0, θ_0) with $r_0 = 0$. Thus, the signals at the receive antennas can be represented by (assuming that $\mathbf{s}(n) = 0$ for $n \leq 0$):

$$\mathbf{x}(n) = \alpha \mathbf{a}_r(\theta_0)\, \mathbf{a}_t(\theta_0)^T\, \mathbf{s}(n)\, e^{j2\pi(n-1)\nu_0} + \mathbf{d}(n) + \mathbf{v}(n), \tag{1}$$

where

- α accounts for the target Radar Cross Section (RCS) with $\mathbb{E}[|\alpha|^2] = \sigma_0^2$. ν_0 is the Doppler frequency of the target.
- $\mathbf{a}_t(\theta_0) \in \mathbb{C}^{N_t \times 1}$ denotes the steering vector and $\mathbf{a}_r(\theta) \in \mathbb{C}^{N_r \times 1}$ is the propagation vector. For simplicity and clearness of expression, both the transmit and receive antennas are assumed to be uniform linear arrays (ULAs) with half-wavelength separation so that

$$\mathbf{a}_t(\theta) = \frac{1}{\sqrt{N_t}} \left[1,\, e^{-j\pi 1 \sin\theta}, \ldots,\, e^{-j\pi(N_t-1)\sin\theta}\right]^T, \tag{2}$$

  and similarly for $\mathbf{a}_r(\theta)$. Please note that the assumption of ULAs is not necessary for this model.
- $\mathbf{d}(n)$ accounts for the the superposition of K signal-dependent uncorrelated point-like interferers. Specifically, the k-th interferer is located at the range-angle position (r_k, θ_k), where $r_k \in \{0, 1, \ldots, N\}$, $\theta_k \in \{0, 1, \ldots, L\} \times \frac{2\pi}{(L+1)}$ with L being the number of discrete azimuth sectors. The received interfering vector $\mathbf{d}(n)$ can be expressed as follows:[2]

$$\mathbf{d}(n) = \sum_{k=1}^{K} \alpha_k \mathbf{a}_r(\theta_k)\, \mathbf{a}_t(\theta_k)^T\, \mathbf{s}(n - r_k)\, e^{j2\pi(n-1)\nu_k}, \tag{3}$$

  where α_k is the complex amplitudes of the k-th interferer with $\mathbb{E}[|\alpha_k|^2] = \sigma_k^2$ and ν_k is its Doppler frequency. Note that the model of $\mathbf{d}(n)$ requires the knowledge of θ_k and α_k for $k = 1, 2, \ldots, K$. This information can be obtained based on a cognitive paradigm by using an environmental dynamic database (EDDB) [37], [50], [51], which includes a geographical information system (GIS), digital terrain maps, previous scanning/acking files, etc. Through the use of geospatial databases and its interaction with RCS clutter models [21], [52, Ch. 15, 16], the location of potentially strong discrete clutter return and its mean power σ_k^2 can be estimated.
- $\mathbf{v}(n)$ denotes the additive Gaussian noise with $\mathbf{v}(n) \sim \mathcal{N}(\mathbf{0},\, \sigma_v^2 \mathbf{I})$.

Let $\mathbf{x} = [\mathbf{x}(1)^T \ldots \mathbf{x}(N)^T]^T$, $\mathbf{s} = [\mathbf{s}(1)^T \ldots \mathbf{s}(N)^T]^T$ and $\mathbf{v} = [\mathbf{v}(1)^T \ldots \mathbf{v}(N)^T]^T$. Expression (1) can be represented as

$$\mathbf{x} = \alpha \mathbf{A}(r_0, \theta_0)\, \mathbf{s} + \sum_{k=1}^{K} \alpha_k \mathbf{A}(r_k, \theta_k)\, \mathbf{s} + \mathbf{v}, \tag{4}$$

where $\mathbf{A}(r_k, \theta_k)$ is determined by the range position r_k and the spatial angle θ_k, given by

$$\mathbf{A}(r_k, \theta_k) = \left[\mathrm{Diag}(\mathbf{p}(\nu_k)) \otimes \left(\mathbf{a}_r(\theta_k)\, \mathbf{a}_t(\theta_k)^T\right)\right] \mathbf{J}_{r_k}, \tag{5}$$

where $\mathbf{J}_{r_k}$ is the shift matrix given by

$$\mathbf{J}_{r_k}(m,n) = \begin{cases} 1, & m - n = N_t \times r_k \\ 0, & m - n \neq N_t \times r_k \end{cases} (m,n) \in \{1, \ldots, N_t N\}^2, \tag{6}$$

and

$$\mathbf{p}(\nu_k) = \left[1, e^{j2\pi\nu_k}, \ldots, e^{j2\pi(N-1)\nu_k}\right]^T \tag{7}$$

with ν_k being the Doppler frequency for $k = 0, 1, \ldots, K$. Hereafter, the Doppler frequencies $\{\nu_k\}_{k=0}^K$ are assumed to be zero without loss of generality (i.e., both the target and the interferers are assumed to be slowly-moving or stay still), and $\mathbf{A}(r_k, \theta_k)$ will be denoted by $\mathbf{A}_k$ for simplicity of notation.

Suppose linear finite impulse response receive filters $\mathbf{w}$ are deployed. Then the output of the filter is given by

$$r = \mathbf{w}^H \mathbf{x} = \alpha \mathbf{w}^H \mathbf{A}_0 \mathbf{s} + \mathbf{w}^H \sum_{k=1}^{K} \alpha_k \mathbf{A}_k \mathbf{s} + \mathbf{w}^H \mathbf{v}. \tag{8}$$

Based on the model, the output SINR is given by

$$\mathrm{SINR} = \frac{\sigma_0^2 \left|\mathbf{w}^H \mathbf{A}_0 \mathbf{s}\right|^2}{\mathbf{w}^H \left(\sum_{k=1}^{K} \sigma_k^2 \mathbf{A}_k \mathbf{s}\mathbf{s}^H \mathbf{A}_k^H\right) \mathbf{w} + \sigma_v^2 \mathbf{w}^H \mathbf{w}}. \tag{9}$$

Thus, the design problem can be formulated from the perspective of maximizing the SINR as follows:

$$\begin{aligned} \underset{\mathbf{s},\, \mathbf{w}}{\text{maximize}} \quad & \frac{\left|\mathbf{w}^H \mathbf{A}_0 \mathbf{s}\right|^2}{\mathbf{w}^H \boldsymbol{\Psi}(\mathbf{s}) \mathbf{w} + \mathbf{w}^H \mathbf{w}} \\ \text{subject to} \quad & \mathbf{s} \in \mathcal{S}, \end{aligned} \tag{10}$$

where $\boldsymbol{\Psi}(\mathbf{s}) = \sum_{k=1}^{K} q_k \mathbf{A}_k \mathbf{s}\mathbf{s}^H \mathbf{A}_k^H$, with positive $q_k = \sigma_k^2 / \sigma_v^2 > 0$, $\mathcal{S} = \{\mathbf{s} | \|\mathbf{s}\|^2 = 1, \mathbf{s} \in \mathcal{S}_c\}$, with $\mathcal{S}_c \in \mathbb{C}^{NN_t}$ denoting a nonempty but not necessarily convex set.

Before proceeding with the design of the solution to problem (10), we address some points of the problem formulation:

- Generally speaking, the problem is hard to solve due to the nonconvex fractional objective, the nonconvex constraint, and the diversity of $\mathcal{S}$.

[2] Strictly speaking, $\mathbf{s}(n - r_k)$ in (3) should be replaced by $\sum_m f_{d_0}(m)\mathbf{s}(n - r_k - m)$ with $f_{d_0}(m)$ the coefficients of the interpolator for the signal shifted by a fraction of the sampling interval d_k. For more details, please refer to [48]. In this work, d_k is assumed to be (approximately) equal to zero for simplicity. If not, the matrix $\mathbf{J}_{r_k}$ shown (6) should be replaced by $\sum_m f_{d_0}(m)\mathbf{J}_{r_k+m}$ in the model. In practice, the integer part r_k can be simply implemented by sample delay while the fractional part d_k would be realized by a FIR fractional delay (FD) filter, which can be designed via many methods [49].

- If the receive filter $\mathbf{w}$ is fixed, problem (10) becomes a waveform design problem which can further be solved by the SDP approach [31], [35], [37]. Thus, it is natural and popular of using the alternating optimization method.
- Problem (10) is a minimum variance distortionless response (MVDR) problem [53] with respect to $\mathbf{w}$. If we already know the optimal sequence $\mathbf{s}$, the optimal receive filter $\mathbf{w}$ will be easily obtained.

III. Algorithmic Framework For Joint Design with Various Sequence Constraints

In this section, we will first introduce the general MM method. Then, based on the MM method, we will derive an algorithmic framework for the joint design problem with simplicity and flexibility to deal with various waveform constraints.

A. Majorization-Minimization Method

The MM method is a powerful optimization scheme, especially when the problem is hard to tackle directly. The idea behind the MM algorithm is to convert the original problem into a sequence of simpler problems to be solved until convergence. The key to using the MM method is to construct a simple majorized problem that can be solved efficiently.

Consider a general optimization problem:

$$\begin{aligned} &\underset{\mathbf{x}}{\text{minimize}} \quad f(\mathbf{x}) \\ &\text{subject to} \quad \mathbf{x} \in \mathcal{X}. \end{aligned} \tag{11}$$

At the ℓ-th iteration, the update rule is

$$\mathbf{x}^{(\ell+1)} \in \underset{\mathbf{x}\in\mathcal{X}}{\operatorname{argmin}}\, u\left(\mathbf{x},\, \mathbf{x}^{(\ell)}\right), \tag{12}$$

where $u(\mathbf{x},\, \mathbf{x}^{(\ell)})$ is a majorizing function (majorizer) of $f(\mathbf{x})$ at $\mathbf{x}^{(\ell)}$.

The convexity of the constraint set $\mathcal{X}$ decides which type of stationary points the MM method converges to. Suppose the constraint set $\mathcal{X}$ is convex. The majorizer must satisfy the following conditions to guarantee the convergence to a d(irectional) stationary point [54]:

$$u(\mathbf{x},\mathbf{y}) \geq f(\mathbf{x}),\ \text{for } \forall \mathbf{x},\mathbf{y} \in \mathcal{X} \tag{13}$$

$$u(\mathbf{y},\mathbf{y}) = f(\mathbf{y}),\ \text{for } \forall \mathbf{y} \in \mathcal{X} \tag{14}$$

$$u'(\mathbf{y},\mathbf{y};\mathbf{d}) = f'(\mathbf{y};\mathbf{d}),\ \text{for } \forall \mathbf{d} \text{ with } \mathbf{y}+\mathbf{d} \in \mathcal{X} \tag{15}$$

$$u(\mathbf{x},\mathbf{y}) \text{ is continuous on } (\mathbf{x},\mathbf{y}), \tag{16}$$

where $f'(\mathbf{y};\mathbf{d})$ is the directional derivative defined as $f'(\mathbf{y};\mathbf{d}) = \lim_{\lambda\to 0} \inf \frac{f(\mathbf{y}+\lambda\mathbf{d})-f(\mathbf{y})}{\lambda}$. In [54], it is proved that the limit point $\mathbf{x}^{(\infty)}$ satisfies

$$f'\left(\mathbf{x}^{(\infty)};\mathbf{d}\right) \leq 0,\ \text{for } \forall \mathbf{d} \text{ with } \mathbf{x}^{(\infty)}+\mathbf{d} \in \mathcal{X}. \tag{17}$$

Thus, $\mathbf{x}^{(\infty)}$ is called the d(irectional) stationary point.

Suppose the constraint set $\mathcal{X}$ is nonconvex. The condition (15) needs to be modified to guarantee the convergence:

$$u'(\mathbf{y},\mathbf{y};\mathbf{d}) = f'(\mathbf{y};\mathbf{d}),\ \text{for } \forall \mathbf{d} \in \mathcal{T}_{\mathcal{X}}(\mathbf{y}), \tag{18}$$

where u and f are defined on the whole $\mathbb{R}$ space and $\mathcal{T}_{\mathcal{X}}(\mathbf{y})$ is the Boulingand tangent cone of $\mathcal{X}$ at $\mathbf{y}$. Following this modification, we can prove that the limit point $\mathbf{x}^{(\infty)}$ satisfies

$$f'\left(\mathbf{x}^{(\infty)};\mathbf{d}\right) \leq 0,\ \text{for } \forall \mathbf{d} \in \mathcal{T}_{\mathcal{X}}\left(\mathbf{x}^{(\infty)}\right). \tag{19}$$

Thus, $\mathbf{x}^{(\infty)}$ is called the B(oulingand) stationary point [55], [56].[3]

One interesting and useful property of MM-based methods is monotonicity:

$$f\left(\mathbf{x}^{(\ell+1)}\right) \leq u\left(\mathbf{x}^{(\ell+1)},\mathbf{x}^{(\ell)}\right) \leq u\left(\mathbf{x}^{(\ell)},\mathbf{x}^{(\ell)}\right) = f\left(\mathbf{x}^{(\ell)}\right), \tag{20}$$

where the first inequality follows from (13), the second one follows from (12), and the last equality follows from (14).

Three points are worth to note here. First, the convergence speed of the MM algorithm is mainly determined by the majorizer, i.e., how closely it resembles the original function. In some cases, if the majorizer is ill-constructed, some acceleration techniques have to be adopted. Second, from (20), we see that even though $\mathbf{x}^{(\ell+1)}$ is not the minimizer of $u(\mathbf{x},\mathbf{x}^{(\ell)})$, the monotonicity can still be guaranteed as long as it improves the function $u(\mathbf{x}^{(\ell+1)},\mathbf{x}^{(\ell)}) \leq u(\mathbf{x}^{(\ell)},\mathbf{x}^{(\ell)})$. Third, the MM algorithm is ready to be implemented with the combination of some acceleration techniques without loss of convergence.[4]

B. Majorized Iteration Method for Joint Design

For a given $\mathbf{s}$, problem (10) with respect to $\mathbf{w}$ can be equivalently reformulated into

$$\begin{aligned} &\underset{\mathbf{w}}{\text{minimize}} \quad \mathbf{w}^H\left[\mathbf{\Psi}(\mathbf{s}) + \mathbf{I}\right]\mathbf{w} \\ &\text{subject to} \quad \mathbf{w}^H\mathbf{A}_0\mathbf{s} = 1, \end{aligned} \tag{21}$$

to which a closed-form solution is given by

$$\mathbf{w}^\star = \frac{\left[\Psi(\mathbf{s}) + \mathbf{I}\right]^{-1}\mathbf{A}_0\mathbf{s}}{\mathbf{s}^H\mathbf{A}_0^H\left[\Psi(\mathbf{s}) + \mathbf{I}\right]^{-1}\mathbf{A}_0\mathbf{s}}. \tag{22}$$

Substituting (22) into (10), and after some algebraic manipulations, problem (10) reduces to

$$\begin{aligned} &\underset{\mathbf{s}}{\text{maximize}} \quad \mathbf{s}^H\left(\mathbf{A}_0^H\left[\Psi(\mathbf{s}) + \mathbf{I}\right]^{-1}\mathbf{A}_0\right)\mathbf{s} \\ &\text{subject to} \quad \mathbf{s} \in \mathcal{S}. \end{aligned} \tag{23}$$

[3]Following the notations and problem settings of [54], the proof mostly follows that of [54, Theorem 1] with only "$z+d \in \mathcal{X}$" replaced by $d \in \mathcal{T}_{\mathcal{X}}(z)$, which is based on [57, Proposition 4.7.1].

[4]The proof of the convergence of the accelerated MM mostly follows that of [54, Theorem 1] with slight modifications on one equation: (following the notations and problem settings of [54]) $u(x,x^{r_j}) \geq u(\mathrm{MM}(x^{r_j}),x^{r_j}) \geq f(\mathrm{MM}(x^{r_j})) \geq f(x^{r_j+1}) \geq f(x^{r_j+1}) \geq u(x^{r_j+1},x^{r_j+1})$, where $MM(\cdot)$ is the MM algorithm mapping and x^{r_j+1} is the next iteration point found by the acceleration technique.

Defining $\mathbf{S}=\mathbf{s}\mathbf{s}^H$, problem (23) is equivalent to

$$\begin{aligned}\underset{\mathbf{s},\mathbf{S}}{\text{minimize}} \quad & -\mathbf{s}^H\left(\mathbf{A}_0^H\left[\Psi\left(\mathbf{S}\right)+\mathbf{I}\right]^{-1}\mathbf{A}_0\right)\mathbf{s}\\ \text{subject to} \quad & \mathbf{S}=\mathbf{s}\mathbf{s}^H\\ & \mathbf{s}\in\mathcal{S},\end{aligned}\tag{24}$$

where $\Psi(\mathbf{S})=\sum_{k=1}^{K}q_k\mathbf{A}_k\mathbf{S}\mathbf{A}_k^H$.

Lemma 1: Denote the objective function of problem (24) by $f(\mathbf{s},\mathbf{S})$. Then, $f(\mathbf{s},\mathbf{S})$ is a concave function of $\mathbf{s}$ and $\mathbf{S}$ jointly, and a majorizer of $f(\mathbf{s},\mathbf{S})$ is

$$\begin{aligned}u_1\left(\mathbf{s},\mathbf{S};\mathbf{s}_\ell,\mathbf{S}_\ell\right)=&-2\,\mathrm{Re}\left(\mathbf{z}_\ell^H\mathbf{s}\right)+2\,\mathrm{Tr}\left(\mathbf{P}_\ell\mathbf{S}\right)\\&-2\,\mathrm{Tr}\left(\mathbf{P}_\ell\mathbf{S}_\ell\right)-f\left(\mathbf{s}_\ell,\mathbf{S}_\ell\right),\end{aligned}\tag{25}$$

where

$$\mathbf{z}_\ell=\mathbf{A}_0^H\left[\Psi\left(\mathbf{S}_\ell\right)+\mathbf{I}\right]^{-1}\mathbf{A}_0\mathbf{s}_\ell,\tag{26}$$

$$\mathbf{P}_\ell=\sum_{k=1}^{K}q_k\left(\mathbf{Q}_\ell^k\right)^H\mathbf{S}_\ell\mathbf{Q}_\ell^k,\tag{27}$$

and

$$\mathbf{Q}_\ell^k=\mathbf{A}_0^H\left[\Psi\left(\mathbf{S}_\ell\right)+\mathbf{I}\right]^{-1}\mathbf{A}_k.\tag{28}$$

Proof: See Appendix A. ■

Ignoring the constant terms and undoing the change of variables $\mathbf{S}=\mathbf{s}\mathbf{s}^H$ in the function (33), the first majorized problem is then given by

$$\begin{aligned}\underset{\mathbf{s}}{\text{minimize}} \quad & \mathbf{s}^H\mathbf{P}_\ell\mathbf{s}-\mathrm{Re}\left(\mathbf{z}_\ell^H\mathbf{s}\right)\\ \text{subject to} \quad & \mathbf{s}\in\mathcal{S}.\end{aligned}\tag{29}$$

Whether problem (29) can be solved efficiently mainly depends on the convexity of the constraint set $\mathcal{S}$ since the objective function is already convex. In the following lemma, we will employ the MM strategy again to further simplify this objective function. The reason we conduct the second majorization is that after simplifying the objective function, closed-form solutions to these subproblems will probably be found for many constraint cases, even nonconvex ones, which will be seen clearly in Section IV.

Conducting the second majorization lowers the complexity at each iteration by finding a probable closed-form solution. At the same time, the second majorizing function might become looser, which consequently increases the number of iterations for the convergence. Thus, there is clearly a trade-off between the complexity of each iteration and the number of iterations. This trade-off reminds us which majorization should be used when dealing with a specific constraint set. In the following, we derive algorithms based on the first majorization and/or the second majorzation, and the trade-off can be reflected clearly in the simulation of the similarity constraint case.

Lemma 2: [14] Let $\mathbf{L}$ be an $n\times n$ Hermitian matrix and $\mathbf{M}$ be another $n\times n$ Hermitian matrix such that $\mathbf{M}\succeq\mathbf{L}$. Then for any point $\mathbf{x}_0\in\mathbf{C}^n$, the quadratic function $\mathbf{x}^H\mathbf{L}\mathbf{x}$ is majorized by $\mathbf{x}^H\mathbf{M}\mathbf{x}+2\,\mathrm{Re}(\mathbf{x}^H(\mathbf{L}-\mathbf{M})\mathbf{x}_0)+\mathbf{x}_0^H(\mathbf{M}-\mathbf{L})\mathbf{x}_0$ at $\mathbf{x}_0$.

By using the above lemma, a majorizer of the objective function of problem (29) can be constructed as follows:

$$\begin{aligned}u_2\left(\mathbf{s},\mathbf{s}_\ell\right)=&\,\lambda_u\left(\mathbf{P}_\ell\right)\mathbf{s}^H\mathbf{s}+2\mathrm{Re}\left(\mathbf{s}^H\left(\mathbf{P}_\ell-\lambda_u\left(\mathbf{P}_\ell\right)\mathbf{I}\right)\mathbf{s}_\ell\right)\\&+\mathbf{s}_\ell^H\left(\lambda_u\left(\mathbf{P}_\ell\right)\mathbf{I}-\mathbf{P}_\ell\right)\mathbf{s}_\ell-\mathrm{Re}\left(\mathbf{z}_\ell^H\mathbf{s}\right),\end{aligned}\tag{30}$$

where $\lambda_u(\mathbf{P}_\ell)$ is an upper bound of the eigenvalues of the positive semidefinite matrix $\mathbf{P}_\ell$, which could be simply chosen as $\mathrm{Tr}(\mathbf{P}_\ell)$ considering the computation cost. Please note that the tightness of the upper bound $\lambda_u(\mathbf{P}_\ell)$ affects the performance of the convergence speed.

Due to $\mathbf{s}^H\mathbf{s}=1$, we have the following second majorized problem:

$$\begin{aligned}\underset{\mathbf{s}}{\text{minimize}} \quad & \mathrm{Re}\left(\mathbf{v}_\ell^H\mathbf{s}\right)\\ \text{subject to} \quad & \mathbf{s}\in\mathcal{S},\end{aligned}\tag{31}$$

where

$$\mathbf{v}_\ell=2\left(\mathbf{P}_\ell-\lambda_u\left(\mathbf{P}_\ell\right)\mathbf{I}\right)\mathbf{s}_\ell-\mathbf{z}_\ell.\tag{32}$$

IV. Four Cases of the Joint Design

In this section, we will consider four waveform constraints: the constant modulus constraint, the similarity constraint, the PAR constraint and the spectral compatibility constraint. For the constant modulus constraint and the PAR constraint, we derive the algorithms based on the second majorization. For the similarity constraint, we derive two algorithms based on the first and second majorizations, respectively. For the spectral compatibility constraint, both the global design and the local design are considered, where the former is based on the first majorization and the latter is based on the second majorization.

A. Constant Modulus Constraint

Note that in practice, due to the limitations of hardware components (such as the maximum signal amplitude clip of A/D converters and power amplifiers), it is usually desirable to transmit constant modulus waveforms. Problem (31) becomes

$$\begin{aligned}\underset{\mathbf{s}}{\text{minimize}} \quad & \mathrm{Re}\left(\mathbf{v}_\ell\mathbf{s}\right)\\ \text{subject to} \quad & |s_n|=\frac{1}{\sqrt{NN_t}},\ \text{for } i=1,\ldots,NN_t,\end{aligned}\tag{33}$$

which has the closed-form solution

$$\mathbf{s}=-e^{j\arg(\mathbf{v}_\ell)}/\sqrt{NN_t},\tag{34}$$

where $e^{j\arg(\cdot)}$ is an element-wise operation.

Note that if the constant modulus constraint in problem (33) is removed from $\mathcal{S}$, we can still obtain the closed-form solution as $\mathbf{s}=-\frac{\mathbf{v}}{\|\mathbf{v}\|}$.

B. Similarity Constraint

Enforcing a similarity constraint introduces a trade-off between maximizing SINR and possessing desirable properties of a known sequence. Thus, the design problem becomes finding waveforms $\mathbf{s}$ in the neighborhood of the reference waveforms

$\mathbf{s}_{\mathsf{ref}}$ to maximize the SINR. The similarity constraint is usually expressed as

$$\|\mathbf{s}-\mathbf{s}_{\mathsf{ref}}\|_\infty \le \epsilon, \tag{35}$$

where $\|\mathbf{s}_{\mathsf{ref}}\|_2 = 1$ and ϵ is within $0 \le \epsilon \le \frac{2}{\sqrt{NN_t}}$ to control the degree of similarity.

1) Method Based on the First Majorization: Note that if the finite energy constraint is reduced to the constant modulus constraint, the similarity constraint can be recast as in [23] and we have the following problem:

$$\begin{aligned} \underset{\mathbf{s}}{\mathsf{minimize}} \quad & \mathbf{s}^H\mathbf{P}_\ell\mathbf{s} - \mathrm{Re}\left(\mathbf{z}_\ell^H\mathbf{s}\right) \\ \mathsf{subject\ to} \quad & |s_n| = \frac{1}{\sqrt{NN_t}} \\ & \arg\left(s_n\right) \in \left[\gamma_n, \gamma_n+\delta\right], \end{aligned} \tag{36}$$

where $\gamma_n = \arg(\mathbf{s}_{\mathsf{ref}}(n)) - \arccos(1-NN_t\epsilon^2/2)$ and $\delta = 2\arccos(1-NN_t\epsilon^2/2)$.

The block coordinate descent method (BCD) can be deployed for problem (36). Assuming all the elements of $\mathbf{s}$, except s_n, are fixed, the problem of s_n is given by

$$\begin{aligned} \underset{s_n}{\mathsf{minimize}} \quad & \mathrm{Re}(a_n^* s_n) \\ \mathsf{subject\ to} \quad & |s_n| = \frac{1}{\sqrt{NN_t}} \\ & \arg\left(s_n\right) \in \left[\gamma_n, \gamma_n+\delta\right], \end{aligned} \tag{37}$$

where

$$a_n = 2\sum_{i=1, i\ne n}^{NN_t} s_i P_{n,i} - z_n, \tag{38}$$

where $P_{n,i}$ is the (n,i)-th entry of $\mathbf{P}_\ell$, and z_n is the n-th element of $\mathbf{z}$. The closed-form solution to problem (37) is already shown in [38] and rewritten as follows:

$$s_n = \begin{cases} \frac{e^{j\gamma_n}}{\sqrt{NN_t}} & \arg(v_n) \in \left[\gamma_n + \frac{\delta}{2} + (2k-2)\pi, \gamma_n + (2k-1)\pi\right] \\ \frac{-e^{j\arg(a_n)}}{\sqrt{NN_t}} & \arg(v_n) \in \left[\gamma_n + (2k-1)\pi, \gamma_n + \delta + (2k-1)\pi\right] \\ \frac{e^{j(\gamma_n+\delta)}}{\sqrt{NN_t}} & \text{otherwise,} \end{cases}$$

where $\exists k \in \mathbb{Z}$, for $n = 1, 2, \ldots, NN_t$. (39)

2) Method Based on the Second Majorization: In this part, we solve the problem based on the second majorization. Thus, the problem becomes

$$\begin{aligned} \underset{\mathbf{s}}{\mathsf{minimize}} \quad & \mathrm{Re}\left(\mathbf{v}_\ell^H\mathbf{s}\right) \\ \mathsf{subject\ to} \quad & |s_n| = \frac{1}{\sqrt{NN_t}} \\ & \arg\left(s_n\right) \in \left[\gamma_n, \gamma_n+\delta\right], \end{aligned} \tag{40}$$

which has a closed-form solution similarly as follows:

$$s_n = \begin{cases} \frac{e^{j\gamma_n}}{\sqrt{NN_t}} & \arg(v_n) \in \left[\gamma_n + \frac{\delta}{2} + (2k-2)\pi, \gamma_n + (2k-1)\pi\right] \\ \frac{-e^{j\arg(v_n)}}{\sqrt{NN_t}} & \arg(v_n) \in \left[\gamma_n + (2k-1)\pi, \gamma_n + \delta + (2k-1)\pi\right] \\ \frac{e^{j(\gamma_n+\delta)}}{\sqrt{NN_t}} & \text{otherwise,} \end{cases}$$

where $\exists k \in \mathbb{Z}$, for $n = 1, 2, \ldots, NN_t$. (41)

C. Peak-to-Average Power Ratio Constraint

The PAR constraint is a relaxed constraint in the practical sense, although mathematically a more general one, as the unimodular case is just a particular case. Imposing the PAR constraint introduces a trade-off between the SINR and the PAR level. The PAR constraint is usually expressed as

$$\mathrm{PAR} = \frac{\max\limits_{1\le n\le NN_t}\left\{|s_n|^2\right\}}{\frac{1}{NN_t}\|\mathbf{s}\|^2} \le \epsilon, \tag{42}$$

where ϵ is the parameter controlling the acceptable level of PAR with $1 \le \epsilon \le NN_t$.

After considering the PAR constraint, let $\gamma = \frac{\epsilon}{NN_t}$, and the problem becomes

$$\begin{aligned} \underset{\mathbf{s}}{\mathsf{minimize}} \quad & \mathrm{Re}\left(\mathbf{v}_\ell\mathbf{s}\right) \\ \mathsf{subject\ to} \quad & \|\mathbf{s}\|^2 = 1 \\ & |s_n| \le \sqrt{\gamma}, \end{aligned} \tag{43}$$

Lemma 3: Without loss of generality, we assume that $|v_1| \ge |v_2| \ge \cdots \ge |v_N|$ and the number of nonzero elements of $\mathbf{v}$ is m. Then the solution to problem (43) is as follows:

$$\mathbf{s} = \mathcal{P}_{\mathcal{S}}\left(\mathbf{v}\right), \tag{44}$$

where

$$\begin{aligned} \mathcal{P}_{\mathcal{S}}\left(\cdot\right) = & -\left(\mathbf{1}_{\mathbb{R}_{\ge 0}}\left(1-m\gamma\right)\right)\sqrt{\gamma}\mathbf{u}_m \odot e^{jarg(\cdot)} \\ & -\left(\mathbf{1}_{\mathbb{R}_{<0}}\left(1-m\gamma\right)\right)\min\{\beta|\mathbf{v}|, \sqrt{\gamma}\mathbf{1}\} \odot e^{jarg(\cdot)}, \end{aligned} \tag{45}$$

$\min\{\cdot,\cdot\}$, $|\cdot|$ and $e^{jarg(\cdot)}$ are element-wise operations,

$$\mathbf{1}_A\left(x\right) = \begin{cases} 1, & \text{if } x \in A, \\ 0, & \text{otherwise,} \end{cases} \tag{46}$$

$$\mathbf{u}_m = \left[\underbrace{1, \ldots 1}_{m}, \underbrace{\sqrt{\frac{1-m\gamma}{NN_t\gamma - m\gamma}}, \ldots, \sqrt{\frac{1-m\gamma}{NN_t\gamma - m\gamma}}}_{NN_t - m}\right]^T,$$

and

$$\begin{aligned} \beta \in \Bigg\{ \beta \Bigg| & \sum_{n=1}^{N} \min\left\{\beta^2\left|v_n\right|^2, \gamma\right\} \\ & = 1, \beta \in \left[0, \frac{\sqrt{\gamma}}{\min\{|v_n||v_n| \ne 0\}}\right] \Bigg\}. \end{aligned} \tag{47}$$

Proof: A similar proof has been given in [58]. For details please refer to [58, Algorithm 2]. ■

D. Spectral Compatibility Constraint

The interference control for the coexistence has been extensively researched in cognitive radio [59], [60] and also applies to the radar field. In order to control the interference brought to the coexisting telecommunication systems, the spectral compatibility constraint is imposed to introduce a trade-off between the SINR and the power spectral density (PSD).

The spectral compatibility constraint is given by [40]

$$\mathbf{c}^H \mathbf{R} \mathbf{c} \leq E_I, \tag{48}$$

where $\mathbf{c}$ is a transmitted coherent burst of N sub-pulses, and E_I is the maximum allowed interference; the spectral compatibility matrix is defined as

$$\mathbf{R} = \sum_{i=1}^{M} \omega_i \mathbf{R}_i, \tag{49}$$

where ω_i is the weight corresponding to the i-th coexisting wireless network; and

$$\mathbf{R}_i(m,l) = \begin{cases} f_{upper}^i - f_{lower}^i & \text{if } m = l \\ \frac{e^{j2\pi f_2^i (m-l)} - e^{j2\pi f_1^i (m-l)}}{j2\pi (m-l)} & \text{if } m \neq l, \end{cases} \tag{50}$$

where f_{lower}^i and f_{upper}^i denote the lower and upper normalized frequencies for the i-th wireless network, respectively. Thus, $\mathbf{c}^H \mathbf{R}_i \mathbf{c}$ represents the energy of the radar system transmitted on the i-th band $[f_{lower}^i, f_{upper}^i]$, and consequently, $\mathbf{c}^H \mathbf{R} \mathbf{c}$ represents the total weighted energy of the sequence $\mathbf{c}$ transmitted on all M bands.

1) Global Design for Spectral Compatibility: Recall that in the model, $\mathbf{s}$ consists of the N_t waveforms with $\mathbf{s} = [\mathbf{s}(1)^T \ldots \mathbf{s}(N)^T]^T$, where $\mathbf{s}(n) \in \mathbb{C}^{N_t \times 1}$ for $n = 1, \ldots, N$. Thus, the waveform transmitted by the k-th antenna is given by

$$\mathbf{s}_k = \left[\mathbf{s}(1,k)^T \ldots \mathbf{s}(N,k)^T\right]^T \text{ for } k = 1, 2, \ldots, N_t, \tag{51}$$

where $\mathbf{s}(i,k)$ represents the k-th element of $\mathbf{s}(i)$. The k-th waveform can be expressed as

$$\mathbf{s}_k = (\mathbf{I}_N \otimes \mathbf{u}_k)\, \mathbf{s} = \mathbf{U}_k \mathbf{s}, \tag{52}$$

where $\mathbf{u}_k = [\overbrace{0, \ldots, 0}^{k-1}, 1, \overbrace{0, \ldots, 0}^{N_t - k}]$ and $k = 1, \ldots, N_t$. Thus, the spectrum compatibility constraint for global design is expressed as

$$\mathbf{s}^H \left(\mathbf{U}_1^H \mathbf{R} \mathbf{U}_1 + \ldots + \mathbf{U}_{N_t}^H \mathbf{R} \mathbf{U}_{N_t}\right) \mathbf{s} = \mathbf{s}^H \widetilde{\mathbf{R}} \mathbf{s} \leq E_I, \tag{53}$$

where $\mathbf{R}$ is defined in (49). The inequality (53) means that the total energy of all the N_t transmit waveforms on those M bands is no more than a threshold. Therefore, the optimization problem based on the first majorization is formulated as

$$\begin{aligned} \underset{\mathbf{s}}{\text{minimize}} \quad & \mathbf{s}^H \mathbf{P}_\ell \mathbf{s} - \text{Re}\left(\mathbf{z}_\ell^H \mathbf{s}\right) \\ \text{subject to} \quad & \|\mathbf{s}\|^2 = 1 \\ & \mathbf{s}^H \widetilde{\mathbf{R}} \mathbf{s} \leq E_I, \end{aligned} \tag{54}$$

where the maximum allowed interference E_I is with $\lambda_{\min}(\widetilde{\mathbf{R}}) \leq E_I \leq \lambda_{\max}(\widetilde{\mathbf{R}})$.

Note that problem (54) can be equivalently reformulated as an rank-one constrained SDP problem, which can be further solved by SDR [61]. According to [62], there must exist a rank-one solution for the SDR problem. Thus, the rank-constrained solution procedure I proposed in [63] can be deployed to reconstruct the global optimal $\mathbf{s}$. However, this approach can guarantee the optimality of the solution but at the cost of long running time. In the context of radar application with emphasis on real-time capability, a fast-solving approach is desired as long as the solution is suboptimal or good enough.

It is obvious that the constraint $\|\mathbf{s}\|^2 = 1$ can be equivalently rewritten as $1 \leq \|\mathbf{s}\|^2 \leq 1$. After this reformulation, the FPP-SCA algorithm [64] can be applied. At the k-th iteration of the FPP-SCA algorithm, we need to solve the following problem

$$\begin{aligned} \underset{\mathbf{s},t}{\text{minimize}} \quad & \mathbf{s}^H \mathbf{P}_\ell \mathbf{s} - \text{Re}\left(\mathbf{z}_\ell^H \mathbf{s}\right) + \mu\varepsilon \\ \text{subject to} \quad & \|\mathbf{s}\|^2 \leq 1 + \varepsilon \\ & \mathbf{s}_k^H \mathbf{s}_k - 2\text{Re}\left(\mathbf{s}_k^H \mathbf{s}\right) \leq \varepsilon - 1 \\ & \mathbf{s}^H \widetilde{\mathbf{R}} \mathbf{s} \leq E_I \\ & \varepsilon \geq 0, \end{aligned} \tag{55}$$

where μ is the penalty parameter to scale the impact of the penalty term.

Note that due to the slack variable ε, problem (55) is always feasible and being a convex QCQP, which can be solved efficiently by off-the-shelf solvers, e.g., MOSEK [65]. In order to guarantee the feasibility of the solution to the original problem, a large parameter μ is suggested in [64] to force the slack variable toward zero. In terms of convergence, if FPP-SCA converges, it converges to the KKT point of problem (55). Further, if the converged slack variable ε is zero, then the remaining variable $\mathbf{s}$ is the KKT point of problem (54).

2) Local Design for Spectral Compatibility: Note that formulation (54) can only guarantee that the total energy on these frequency intervals is below a threshold without discrimination on the these intervals. However, in some application scenarios, the priority of some frequency interval is higher than the others because of the commercial or military purpose. In order to obtain waveforms with satisfactory PSDs for these application scenarios, we focus on designing the N_t waveforms separately. The optimization problem is formulated as

$$\begin{aligned} \underset{\{\mathbf{s}_k\}_{k=1}^{N_t}}{\text{minimize}} \quad & \text{Re}\left(\mathbf{v}_\ell^H \mathbf{s}\right) \\ \text{subject to} \quad & \|\mathbf{s}_k\|^2 = \frac{1}{N_t} \\ & \mathbf{s}_k^H \mathbf{R}_i \mathbf{s}_k \leq E_i, \text{ for } i = 1, \ldots, M \\ & \mathbf{s}_k = \left[\mathbf{s}(1,k)^T \ldots \mathbf{s}(N,k)^T\right]^T, \end{aligned} \tag{56}$$

where $\mathbf{R}_i$ is defined as (49) and E_i is the maximum allowed interference with $\lambda_{\min}(\mathbf{R}_i) \leq E_i \leq \lambda_{\max}(\mathbf{R}_i)$.

Since the objective function is linear on $\{\mathbf{s}_k\}_{k=1}^{N_t}$, problem (56) can be decomposed into N_t subproblems as follows:

$$\begin{aligned} \underset{\mathbf{s}_k}{\text{minimize}} \quad & \mathrm{Re}\left(\left(\mathbf{v}_\ell^k\right)^H \mathbf{s}_k\right) \\ \text{subject to} \quad & \|\mathbf{s}_k\|^2 = \frac{1}{N_t} \\ & \mathbf{s}_k^H \mathbf{R}_i \mathbf{s}_k \le E_i, \text{ for } i = 1, \ldots, M, \end{aligned} \tag{57}$$

where $\mathbf{v}_\ell^k = [v(k), v(k+N_t), \ldots, v(k+(N-1)N_t)]^T$.

First, note that all the N_t subproblems can be solved in parallel. This parallel computing is only possible after the second majorization. Second, problem (57) has $(m+1)$ quadratic constraints, which brings up the feasibility issue. The feasibility of problem (57) depends on whether the feasible set of the M inequality constraints has an nonempty intersection with the equality constraint. However, establishing (in)feasibility of an optimization problem is generally NP-hard. Instead of studying the feasibility of this problem before solving it, we use the FPP technique [64] directly on problem (57), which is similar to the counterpart of the global design case and thus omitted. The problem after using the FPP-SCA technique is always feasible. As argued in [64], if $(\mathbf{s}_k^\star, \varepsilon_k^\star)$ with $\varepsilon^\star$ being the optimal slack variable is the optimal solution and $\varepsilon_k^\star = 0$, then $\mathbf{s}^\star$ is an optimal solution for problem (56). Otherwise, a compromise has to be made to minimize constraint violations in the sense of engineering application. In our case, if $\varepsilon^\star$ is nonzero, we change $\|\mathbf{s}_k\|^2 = \frac{1}{N_t}$ into $\|\mathbf{s}_k\|^2 = \frac{1}{N_t} + \varepsilon_k^\star$. This means that the transmit energy should be tuned from 1 to $1 + \sum_{k=1}^{N_t} \varepsilon_k^\star$ to satisfy the spectrum compatibility constraints, which we believe is much easier than choosing a well-selected $\{E_i\}_{i=1}^M$ for feasibility. In addition, note that our proposed algorithm is ready for this modification because changing $\|\mathbf{s}_k\|^2 = \frac{1}{N_t}$ into $\|\mathbf{s}_k\|^2 = \frac{1}{N_t} + \varepsilon^\star$ has no effect on its derivation.

E. Summary of Algorithm and Complexity Analysis

To summarize, the description of the algorithm with respect to the above constraints is given in Algorithm 1. Hereafter, we use **MIA-CMC**, **MIA-CMSC**, **MIA-PC** and **MIA-SCC**to denote the proposed **M**ajorized **I**terative **A**lgorithm with the **C**onstant **M**odulus **C**onstraint, **C**onstant **M**odulus and **S**imilarity **C**onstraint, PAR **C**onstraint and **S**pectrum **C**ompatibility **C**onstraint, respectively. **MIA-CMSC** can be subdivided into **MIA-CMSC1** (MIA-CMSC based on the first majorization) and **MIA-CMSC2** (MIA-CMSC based on the second majorization). **MIA-SCC** can also be subdivided into **MIA-SCCG** (**MIA-SCC** for **G**lobal design) and **MIA-SCCL** (**MIA-SCC** for **L**ocal design).

We now analyze the computational complexity of the MIA-based algorithms. The overall complexity of each MIA-XXX method is linear with respect to the number of iterations. For the convenience of analysis, we focus on the deterministic cost on a per-iteration basis, which comes from the following three sources: $\mathbf{z}_\ell$, $\mathbf{P}_\ell$, and $\mathbf{s}_{\ell+1}$. The computational cost of $\mathbf{z}_\ell$ is $\mathcal{O}((N_r N)^3)$ because of the inversion operation. With $[\Psi(\mathbf{s}) + \mathbf{I}]^{-1}$ already computed, the computational cost of $\mathbf{Q}_\ell^k$ is $\mathcal{O}((N_r N) \cdot (N_t N)^2)$, and thus the computational cost of $\mathbf{P}_\ell$ should be $\mathcal{O}((N_r N) \cdot (N_t N)^2) + \mathcal{O}((N_t N)^3)$. To sum up, $\mathbf{z}_\ell$ and $\mathbf{P}_\ell$ contributes the total amount of complexity $\mathcal{O}(N^3 \cdot (\max\{N_r, N_t\})^3)$, neglecting the lower order terms.

The update of $\mathbf{s}_{\ell+1}$ varies case by case: For MIA-CMC, MIA-CMSC2 and MIA-PAR, the computation cost mainly comes from the computation of $\lambda_u(\mathbf{P}_\ell)$ and $\mathbf{v}_\ell$. The update of $\lambda_u(\mathbf{P}_\ell)$ is simply chosen as $\mathrm{Tr}(\mathbf{P}_\ell)$, so the computation cost is $\mathcal{O}(N_t N)$. The computational cost of $\mathbf{v}_\ell$ is $\mathcal{O}((N_t N)^2)$. For MIA-CMSC1, there are NN_t subproblems due to the BCD scheme, and the computational cost of each subproblem is $\mathcal{O}(N_t N)$ because of the update of a_n. Thus, the total computational cost is $\mathcal{O}((N_t N)^2)$. For MIA-SCCG, MOSEK will reformulate problem (55) into the epigraph form by introducing one more slack

Algorithm 1: Majorized Iterative Algorithm (MIA).

Input: Initial sequence $\mathbf{s}_0$, convergence threshold(s) ε_{obj} (and ε_{slc}) (and penalty paramters μ_0, $\{\mu_0^i\}_{i=1}^{N_t}$)

Output: Designed sequence $\mathbf{s}$ and receive filter $\mathbf{w}$

1: **repeat**

2: $\mathbf{z}_\ell = \mathbf{A}(\theta)^H [\mathbf{\Psi}(\mathbf{S}_\ell) + \mathbf{I}]^{-1} \mathbf{A}(\theta) \mathbf{s}_\ell$

3: $\mathbf{P}_\ell = \sum_{k=1}^K q_k \left(\mathbf{Q}_\ell^k\right)^H \mathbf{S}_\ell \mathbf{Q}_\ell^k$

4:
- (I) **Constant modulus**:
  - update $\lambda_u(\mathbf{P}_\ell)$
  - $\mathbf{v}_\ell = 2(\mathbf{P}_\ell - \lambda_u(\mathbf{P}_\ell)\mathbf{I})\mathbf{s}_\ell - \mathbf{z}_\ell$
  - obtain $\mathbf{s}_{\ell+1}$ according to (34)
- (II-i) **Similarity based on the 1st majorization**:
  - for $n = 1$ to NN_t
    - $a_n = 2\sum_{i=1, i\neq n}^{NN_T} s_i P_{n,i} - z_n$
    - obtain s_n according to (39)
  - end
- (II-ii) **Similarity based on the 2nd majorization**:
  - update $\lambda_u(\mathbf{P}_\ell)$
  - $\mathbf{v}_\ell = 2(\mathbf{P}_\ell - \lambda_u(\mathbf{P}_\ell)\mathbf{I})\mathbf{s}_\ell - \mathbf{z}_\ell$
  - obtain $\mathbf{s}_{\ell+1}$ according to (41)
- (III) **PAR**:
  - update $\lambda_u(\mathbf{P}_\ell)$
  - $\mathbf{v}_\ell = 2(\mathbf{P}_\ell - \lambda_u(\mathbf{P}_\ell)\mathbf{I})\mathbf{s}_\ell - \mathbf{z}_\ell$
  - obtain $\mathbf{s}_{\ell+1}$ according to (45)
- (IV-i) **Global design for spectrum compatibility**:
  - obtain $\mathbf{s}_{\ell+1}$ by solving the QCQP (55)
  - if $t > \varepsilon_{slc}$: $\mu_{\ell+1} = 2\mu_\ell$; else: $\mu_{\ell+1} = \mu_\ell$
- (IV-ii) **Local design for spectrum compatibility**:
  - obtain $\mathbf{s}_{\ell+1}$ by solving the N_t QCQPs
  - based on problem (57) in parallel
  - if $t_i > \varepsilon_{slc}$: $\mu_{\ell+1}^i = 2\mu_\ell^i$; else: $\mu_{\ell+1}^i = \mu_\ell^i$

5: $\ell \leftarrow \ell + 1$

6: **until**
- (I,II,III): $|f(\mathbf{s}_\ell) - f(\mathbf{s}_{\ell-1})| \le \varepsilon_{obj}$
- (IV-i) : $|f(\mathbf{s}_\ell) - f(\mathbf{s}_{\ell-1})| \le \varepsilon_{obj}$ & $t \le \varepsilon_{slc}$
- (IV-ii) : $|f(\mathbf{s}_\ell) - f(\mathbf{s}_{\ell-1})| \le \varepsilon_{obj}$ & $\{t_i \le \varepsilon_{slc}\}_{i=1}^{N_t}$

7: $\mathbf{w} = \frac{[\Psi(\mathbf{s}_\ell)+\mathbf{I}]^{-1}\mathbf{A}(\theta)\mathbf{s}_\ell}{\mathbf{s}_\ell^H \mathbf{A}(\theta)^H [\Psi(\mathbf{s}_\ell)+\mathbf{I}]^{-1}\mathbf{A}(\theta)\mathbf{s}_\ell}$

variable. Then, there is one linear constraint and three second order cone (SOC) constraints. The computational complexity of solving the problem should be upper bounded by $\mathcal{O}((N_t N)^{3.5})$, the same order as second order cone programming (SOCP). Similarly, the complexity of each subproblem of MIA-SCCL is also upper bounded by $\mathcal{O}(N^{3.5})$. Since there are N_t SOCP subproblems, the computational cost is upper bounded by $\mathcal{O}(N_t \cdot N^{3.5})$.

V. Connection and Comparison With the Alternating Optimization Method

Given that many works address the joint design problem through the alternating optimization approach, in this section, we will first interpret the alternating optimization method from an MM perspective, and then we will reveal the connection and the difference between the alternating optimization method and the MIA.

The alternating optimization method yields the following update rules:

$$\mathbf{w}_{\ell+1} = \arg\max_{\mathbf{w}} \frac{\mathbf{w}^H\left(\mathbf{A}_0 \mathbf{s}\mathbf{s}^H \mathbf{A}_0^H\right)\mathbf{w}}{\mathbf{w}^H\left(\mathbf{\Psi}\left(\mathbf{s}\right)+\mathbf{I}\right)\mathbf{w}} = \alpha\left[\Psi\left(\mathbf{s}_\ell\right)+\mathbf{I}\right]^{-1}\mathbf{A}_0\mathbf{s}_\ell,$$

$$\mathbf{s}_{\ell+1} = \arg\max_{\mathbf{s}\in\mathcal{S}} \frac{\mathbf{s}^H\left(\mathbf{A}_0^H \mathbf{w}_{\ell+1}\mathbf{w}_{\ell+1}^H \mathbf{A}_0\right)\mathbf{s}}{\mathbf{s}^H\left(\mathbf{\Phi}\left(\mathbf{w}_{\ell+1}\right)+\mathbf{w}_{\ell+1}^H\mathbf{w}_{\ell+1}\mathbf{I}\right)\mathbf{s}}. \tag{58}$$

where α is a scalar that does not affect the optimality, and $\mathbf{\Phi}(\mathbf{w}) = \sum_{k=1}^{K} q_k \mathbf{A}_k^H \mathbf{w}\mathbf{w}^H \mathbf{A}_k$.

It is popular to recast the problem with respect to $\mathbf{s}$ into a rank-one constrained SDP problem and then resort to SDR and some rank-one reconstruction technique. If the update rule of $\mathbf{w}_{\ell+1}$ is substituted into that of $\mathbf{s}_{\ell+1}$, the equivalent update rule for problem (10) is given by:

$$\mathbf{s}_{\ell+1} = \arg\min_{\mathbf{s}\in\mathcal{S}} \frac{-\mathbf{s}^H\mathbf{A}_0^H\left[\mathbf{\Psi}\left(\mathbf{s}_\ell\right)+\mathbf{I}\right]^{-1}\mathbf{A}_0\mathbf{s}_\ell\mathbf{s}_\ell^H\mathbf{A}_0^H\left[\mathbf{\Psi}\left(\mathbf{s}_\ell\right)+\mathbf{I}\right]^{-1}\mathbf{A}_0\mathbf{s}}{\mathbf{s}_\ell^H\mathbf{A}_0^H\left[\mathbf{\Psi}\left(\mathbf{s}_\ell\right)+\mathbf{I}\right]^{-1}\left[\mathbf{\Psi}\left(\mathbf{s}\right)+\mathbf{I}\right]\left[\mathbf{\Psi}\left(\mathbf{s}_\ell\right)+\mathbf{I}\right]^{-1}\mathbf{A}_0\mathbf{s}_\ell}. \tag{59}$$

Proposition 4: Denote the objective functions of problem (59) and problem (24) by $u_{alt}(\mathbf{s},\mathbf{s}_\ell)$ and $f(\mathbf{s})$, respectively. Then, $u_{alt}(\mathbf{s},\mathbf{s}_\ell)$ is a majorizer of $f(\mathbf{s})$.

Proof: See Appendix B. ■

Since $\mathbf{S} = \mathbf{s}\mathbf{s}^H$, $u_{alt}(\mathbf{s},\mathbf{s}_\ell)$ can be viewed equivalently as a function of $\mathbf{s}$ and $\mathbf{S}$, denoted as $u_{alt}(\mathbf{s},\mathbf{S};\mathbf{s}_\ell,\mathbf{S}_\ell)$. The connection between $u_{alt}(\mathbf{s},\mathbf{s}_\ell)$ and our first majorizer $u_1(\mathbf{s},\mathbf{S};\mathbf{s}_\ell,\mathbf{S}_\ell)$ is given in the following proposition.

Proposition 5: The function $u_1(\mathbf{s},\mathbf{S};\mathbf{s}_\ell,\mathbf{S}_\ell)$ is a majorizer of $u_{alt}(\mathbf{s},\mathbf{S};\mathbf{s}_\ell,\mathbf{S}_\ell)$.

Proof: See Appendix C. ■

The connection among the original objective function $f(\mathbf{s})$, the equivalent majorizer of the alternating optimization method $u_{alt}(\mathbf{s},\mathbf{s}_\ell)$, the first majorizer $u_1(\mathbf{s},\mathbf{S};\mathbf{s}_\ell,\mathbf{S}_\ell)$, and the second majorizer $u_2(\mathbf{s},\mathbf{s}_\ell)$ is illustrated graphically in Fig. 1. Note that the connections shown in Fig. 1 are based on the fact that a closed-form solution of $\mathbf{w}$ can be found. The alternating optimization approach also allows forcing suitable constraints on $\mathbf{w}$ while it will become difficult to apply the proposed approach if the closed-form solution of $\mathbf{w}$ is hard to be obtained.

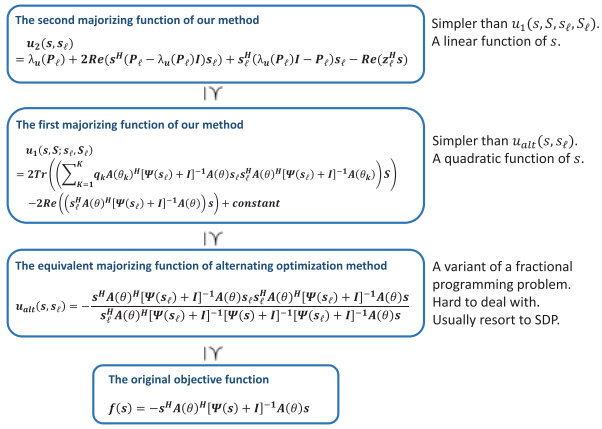

Fig. 1. Connections among the original objective function $f(\mathbf{s})$ and the majorizers $u_{alt}(\mathbf{s},\mathbf{s}_\ell)$,$u_1(\mathbf{s},\mathbf{S};\mathbf{s}_\ell,\mathbf{S}_\ell)$ and $u_2(\mathbf{s},\mathbf{s}_\ell)$.

VI. Numerical Experiments

In this section, we conduct numerical simulations to evaluate the proposed algorithms for the joint design problem. Assume that both the transmitter and receiver are ULAs with half-wavelength separation, $N_t = 8$, $N_r = 8$, and $N = 20$. A target is located at the range-angle position $(0, 15^\circ)$ with power $|\alpha_0|^2 = 20$ dB, and three fixed interferers are located at the range-angle positions $(0, -50^\circ)$, $(1, -10^\circ)$, and $(2, 40^\circ)$, respectively. The power for each interferer is $|\alpha_i|^2 = 20$ dB, for $i = 1, 2, 3$. The noise variance is $\sigma_\nu^2 = 0$ dB. The orthogonal linear frequency modulation (LFM) waveforms are set as the initial and also the reference waveforms for MIA-CMC, MIA-CMSC, and MIA-PC. Denote the space-time sequence matrix of the LFM waveform by $\mathbf{S}_0$. The (k,n)-th entry of $\mathbf{S}_0$ is given by

$$\mathbf{S}_0(k,n) = \frac{1}{\sqrt{NN_t}} \exp\left\{j2\pi\left(n-1\right)\left(k+n-1\right)/N\right\}, \tag{60}$$

where $k = 1,\ldots,N_t$ and $n = 1,\ldots,N$. The initial sequence $\mathbf{s}_0 \in \mathbb{C}^{NN_t\times 1}$ is obtained by stacking the columns of $\mathbf{S}_0$. The initial filter $\mathbf{w}_0$ is obtained according to (14) by using $\mathbf{s}_0$. Unless otherwise specified, all the parameters are the same in the numerical experiments. In the following experiment, we also implement the accelerated version of the corresponding MIA-type method, denoted by MIA-XXX-Accelerated. SQUAREM [66], as an off-the-shelf acceleration scheme, is deployed as the acceleration scheme. All experiments were carried out on a Windows laptop with a 2.60 GHz i7-5600U CPU and 8 GB RAM.

A. Joint Design With the Constant Modulus Constraint

The benchmark methods for the constant modulus constraint are SOA1-CMC (sequential optimization algorithms 1 with constant modulus constraint) and SOA2-CMC (sequential

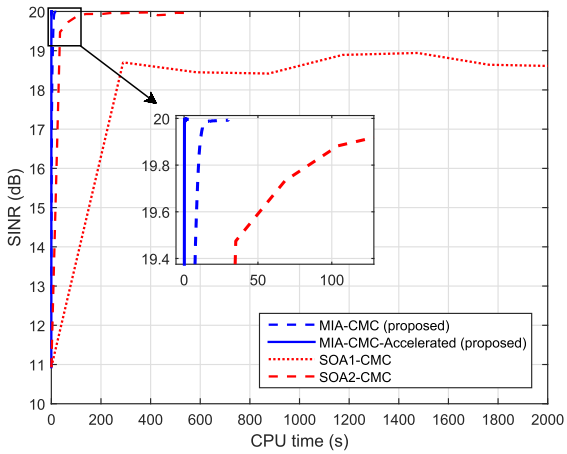

Fig. 2. Convergence plot: SINR versus CPU time for the constant modulus case.

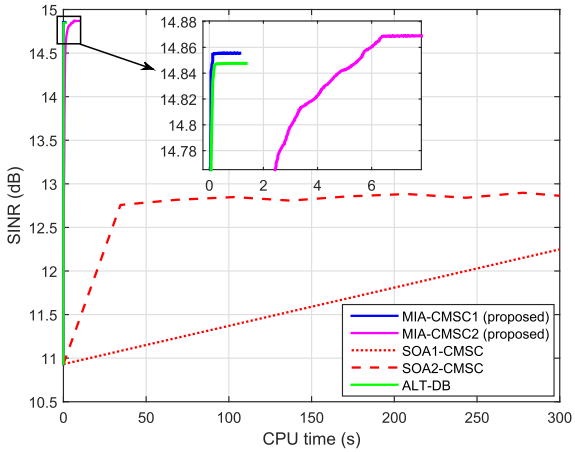

Fig. 4. Convergence plot: SINR versus CPU time for the similarity case. Similarity parameter: $\epsilon = 1/\sqrt{NN_t}$.

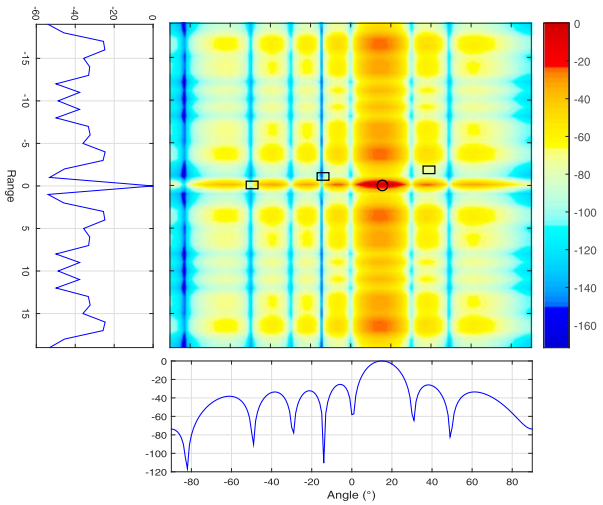

Fig. 3. Range-angle cut of the MIMO ambiguity function for the constant modulus case.

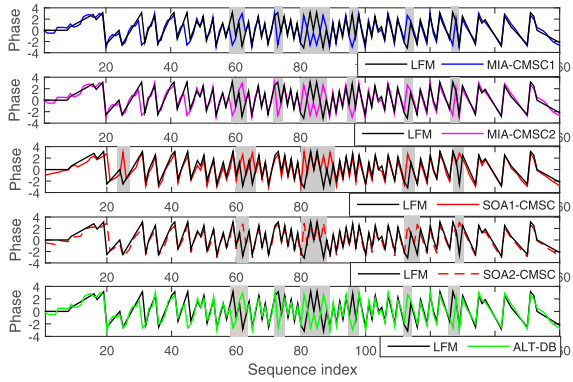

Fig. 5. Comparison of the phase of the reference and designed waveforms.

optimization algorithms 2 with constant modulus constraint) [31]. Both of them employ the SDR and randomization to solve the rank-one constrained SDP problems iteratively.

In Fig. 2, we can see clearly that an obvious advantage of the MIA-type methods is the guarantee of monotonicity, compared with the fluctuation of the SINR achieved by the SOA methods. Besides, both MIA-CMC and MIA-CMC-Accelerated are much faster than the SOA-type methods in terms of the CPU time.

Fig. 3 shows the range-angle cut of the normalized MIMO ambiguity function [67], [68], where rectangle and ellipse represent the locations of interferer and target, respectively. We can see that the energy peak is located in the ellipse, while the energy nulls are located in the rectangles. Fig. 3 also provides the angle cut at the range $r = 0$ and the range cut at the angle $\theta = 15^\circ$. In the range cut, there is a pitfall for the ranges $r = 1$ and $r = 2$. For the beampattern, there is a peak located at the target angle of 15° in the angle cut. Based on our simulation results, the ambiguity functions designed via the proposed algorithms for other constraint cases are also well-shaped. Thus, in the following experiments for other constraints, we focus on the algorithm computational performance and the properties of the designed sequence.

B. Joint Design With the Similarity Constraint

The benchmarks are SOA1-CMSC (sequential optimization algorithms 1 with constant modulus and similarity constraints), SOA2-CMSC (sequential optimization algorithms 2 with constant modulus and similarity constraints) [31], and Algorithm 2 in [51] named ALT-DB here. SOA1-CMSC and SOA2-CMSC are similar to SOA1-CMC and SOA2-CMC, respectively. ALT-DB deploys the alternating scheme, and for the problem with respect to s, the block coordinate descent method is used within the Dinkelbach framework.

From Fig. 4, we can see that the MIA-type methods and ALT-DB are better than the SOA-type methods in terms of both CPU time and converged SINR. Further, MIA-CMSC2 is slightly better than ALT-DB in terms of the achieved SINR with almost the same performance on CPU time.

In Fig. 5, we compare the designed sequences with the reference LFM sequence. From the comparison, we find that all these designed sequences are similar to the reference sequence although there are some small mismatches.

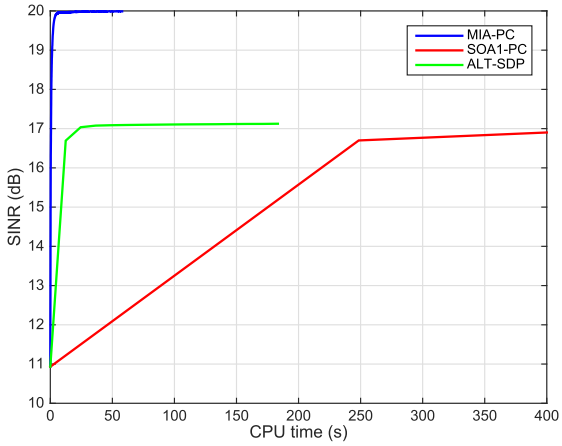

Fig. 6. Convergence plot: SINR versus CPU time for the PAR case. PAR parameter: $\gamma = 0.5$.

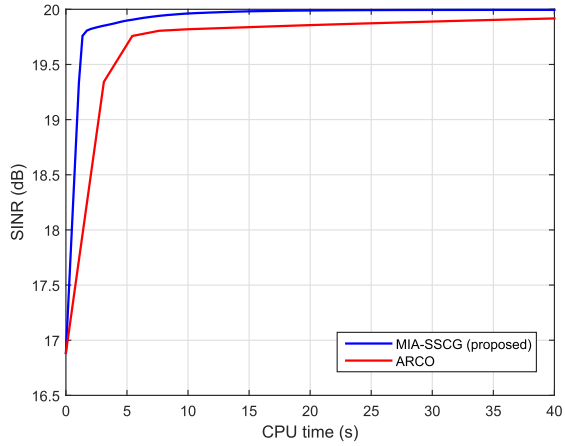

Fig. 7. Convergence plot for the global design: SINR versus CPU time for the spectrum compatibility case with. Total allowed interference: $E_I = (|\lambda_{\max}(\mathbf{R}_2) + \lambda_{\min}(\mathbf{R}_2)| + |\lambda_{\max}(\mathbf{R}_1) + \lambda_{\min}(\mathbf{R}_1)|) \times 10^{-4}$.

C. Joint Design with the PAR Constraint

The SOA1-type method is modified and named SOA1-PC to be a benchmark for the PAR case. The other benchmark is the method proposed in [69] named ALT-SDP here. ALT-SDP can be decomposed into two steps: SDPs of $\mathbf{w}$ and $\mathbf{s}$ are solved alternately in the first step, and $\mathbf{w}$ and $\mathbf{s}$ are synthesized by randomization in the second step. In the experiment about computation efficiency, we only consider the the first step of ALT-SDP. Note that the SINR achieved after the second step may be smaller than that obtained in the first step, and the running time should include the time for the synthesis stage.

Fig. 6 shows that the converged SINR achieved by MIA-PC is about 3 dB higher than SOA1-PC and 5.7 dB higher than ALT-SDP. In addition, MIA-PC converges much faster in terms of CPU time.

D. Joint Design With the Spectrum Compatibility Constraint

The experiment settings are as follows: $N = 40$, $N_t = 2$ and $N_r = 4$. For local design, two frequency intervals are considered. The first frequency interval is $[f^1_{lower}, f^1_{upper}] = [0.2, 0.3]$, together with the spectral compatibility matrix $\mathbf{R}_1$ and the maximum allowed interference E_1. The second frequency interval is $[f^2_{lower}, f^2_{upper}] = [0.75, 0.85]$, together with the spectral compatibility matrix $\mathbf{R}_2$ and the maximum allowed interference E_2. For global design, the spectral compatibility matrix is $\widetilde{\mathbf{R}} = \sum_{k=1}^{N_t} \mathbf{U}_k^H \mathbf{R}_k \mathbf{U}_k$, and the total allowed interference is E_I. The benchmark is the method proposed in [41] named ARCO here.

For the global design of the the spectrum compatibility case, Fig. 7 show the convergence curves. We can see that our method is faster than the benchmark although both methods converges to almost the same SINR. In addition, the averaged PSD's designed by these two methods are compared in Fig. 8, where two deep nulls of the PSD designed by MIA-SCCG are much deeper than the counterparts designed by the benchmark.

Further, we show the effect of the parameter E_I in Fig. 9. With respect to different values of E_I, the achieved SINR's for both MIA-SCCG and ARCO are almost constant. However,

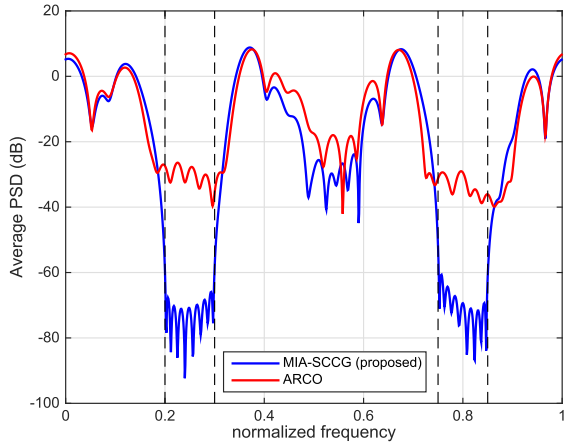

Fig. 8. Comparison of the average PSD of the designed waveforms for the global design. Paremeter settings: $E_I = |\lambda_{\max}(\mathbf{R}_1) + \lambda_{\min}(\mathbf{R}_1)| \times 10^{-4} + |\lambda_{\max}(\mathbf{R}_2) + \lambda_{\min}(\mathbf{R}_2)| \times 10^{-4}$.

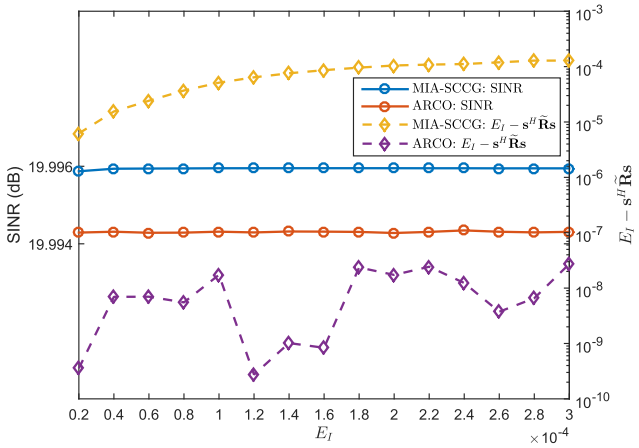

Fig. 9. The effect of E_I on the achieved SINR.

the values of $E_I - \mathbf{s}^H\widetilde{\mathbf{R}}\mathbf{s}$ are quiet different. Specifically, The value of $E_I - \mathbf{s}^H\widetilde{\mathbf{R}}\mathbf{s}$ of ARCO is smaller than that of MIA-SCCG by about five orders of magnitude for each E_I, which means the spectrum compatibility constraint for ARCO is active while it is not active for MIA-SCCG. This supports the re-

TABLE I
COMPARISON OF THE CPU TIME OVER DIFFERENT N

		CPU Time (s)					
		$N = 50$	$N = 100$	$N = 200$	$N = 300$	$N = 400$	$N = 500$
Constant modulus	MIA-CMC	8.1875	52.7813	258.1250	661.7188	1227.7	2088.4
	MIA-CMC-AC	0.2969	0.8438	4.7969	10.7969	23.3594	34.5313
	SOA1-CMC	2084.0	N/A	N/A	N/A	N/A	N/A
	SOA2-CMC	273.7031	N/A	N/A	N/A	N/A	N/A
Similarity	MIA-CMSC1	0.0625	0.3594	1.6563	2.7500	6.4375	10.8281
	MIA-CMSC2	2.8063	17.3594	97.4063	239.0156	464.4531	737.4063
	MIA-CMSC2-AC	0.1875	1.2813	8.6094	23.0938	39.2969	65.9375
	SOA1-CMSC	2089.9	N/A	N/A	N/A	N/A	N/A
	SOA2-CMSC	274.3281	N/A	N/A	N/A	N/A	N/A
	ALT-DB	0.5938	N/A	N/A	N/A	N/A	N/A
PAR	MIA-PC	6.1406	29.7500	138.8438	350.7969	644.6875	1076.3
	MIA-PC-AC	0.2031	0.9531	4.5000	11.4531	20.9844	39.0000
	SOA1-PC	1862.3	N/A	N/A	N/A	N/A	N/A
	ALT-SDP	940.1406	N/A	N/A	N/A	N/A	N/A
Spectrum compatibility	MIA-SCCG	33.4531	46.4875	158.2969	619.4219	718.6406	1325.4
	ARCO	373.4531	N/A	N/A	N/A	N/A	N/A

TABLE II
COMPARISON OF THE SINR OVER DIFFERENT N

		SINR (dB)					
		$N = 50$	$N = 100$	$N = 200$	$N = 300$	$N = 400$	$N = 500$
Constant modulus	MIA-CMC	19.7671	19.7978	19.8030	19.8099	19.8145	19.8174
	MIA-CMC-AC	19.9897	19.9931	19.9952	19.9953	19.9956	19.9957
	SOA1-CMC	17.9972	N/A	N/A	N/A	N/A	N/A
	SOA2-CMC	19.9702	N/A	N/A	N/A	N/A	N/A
Similarity	MIA-CMSC1	16.8102	16.8056	16.8056	16.8062	16.8059	16.8060
	MIA-CMSC2	16.7448	16.7154	16.7485	16.7334	16.7451	16.7360
	MIA-CMSC2-AC	16.8054	16.8061	16.7862	16.7946	16.7281	16.6831
	SOA1-CMSC	14.5997	N/A	N/A	N/A	N/A	N/A
	SOA2-CMSC	15.3144	N/A	N/A	N/A	N/A	N/A
	ALT-DB	16.8088	N/A	N/A	N/A	N/A	N/A
PAR	MIA-PC	19.9309	19.9306	19.9305	19.9305	19.9301	19.9303
	MIA-PC-AC	19.9876	19.9862	19.9855	19.9853	19.9851	19.9853
	SOA1-PC	17.0324	N/A	N/A	N/A	N/A	N/A
	ALT-SDP	14.0359	N/A	N/A	N/A	N/A	N/A
Spectrum compatibility	MIA-SCCG	19.9897	19.9876	19.9860	19.9951	19.9905	19.9909
	ARCO	19.9585	N/A	N/A	N/A	N/A	N/A

sults shown in Fig. 7 and Fig. 8 that MIA-SCCG achieves the SINR as the same as ARCO but with a lower energy threshold E_I.

For the comparison of the global design and local designs, we consider a different scenario, where the spectral requirement on the second frequency interval is relaxed by lifting the maximal allowed interference. Note that the global approach can also be applied to this new scenario indirectly by choosing the appropriate values for ω_i in (49). Fig. 10 shows that the PSD's of the designed waveforms, where the total energy tolerances are the same for both approaches. From this figure, we can see that both approaches emphasize the first interval more than the second one. However, the performance of the MIA-SCCL is better than that of the MIA-SCCG.

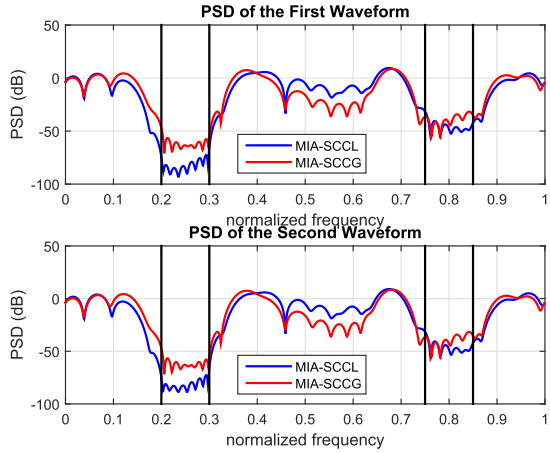

Fig. 10. Comparison of MIA-SCCG and MIA-SCCL. Parameter settings: $E_1 = |\lambda_{\max}(\mathbf{R}_1) + \lambda_{\min}(\mathbf{R}_1)| \times 10^{-4}$, $E_2 = |\lambda_{\max}(\mathbf{R}_2) + \lambda_{\min}(\mathbf{R}_2)| \times 10^{-1}$, $\omega_1 = 100$, $\omega_2 = 0.1$, $E_I = N_t(\omega_1 E_1 + \omega_2 E_2)$.

E. Performance Comparison Over Different N

In the previous sections, we have compared the performance between the proposed MIA and the existing methods for different scenarios for a fixed waveform length N. In this section, we will evaluate these algorithms with respect to different N. The simulation results are shown in Table I and II, where "N/A" is due to the insufficient memory of the experiment laptop. Note

that for the alternating SDP approaches, the CPU time will increase vastly for $N \geq 100$ because they require the complexity $\mathcal{O}((N_t N)^3 + (N_t N)^{6.5})$ per iteration, and the PC we use runs out of memory. Thus, we only provide the results of these benchmarks for the case $N = 50$. From the tables, we can see that the MIA, especially the accelearated version, can be applied to design long sequences considering the performance on both time and SINR.

VII. Conclusion

In this paper, we consider the joint design problem for a colocated MIMO radar, which is formulated as maximizing the SINR subject to multiple waveform constraints. We have derived an efficient and flexible algorithmic framework called MIA (Majorized Iterative Algorithm) on the MM method, which can handle multiple waveform constraints. Specifically, closed-form solutions can be obtained at each iteration if the constant modulus, similarity, or PAR constraint is considered. For the spectrum compatibility constraint, both the local and global designs are considered and the FPP-SCA is applied. In addition, all the derived algorithms can guarantee monotonicity and have lower computational complexity at each iteration compared with the the alternating SDP approach. Numerical experiments show the good performance of MIA under the above four constraints and emphasize its efficiency in terms of the achieved SINR and the CPU time.

Appendix

A. Proof of Lemma 1

Proof: Denote the objective function of (24) by $f(\mathbf{s}, \mathbf{S})$ and define $g(\mathbf{x}, \mathbf{Y}) = \mathbf{x}^H \mathbf{Y}^{-1} \mathbf{x}$, where $\mathbf{Y} \succ \mathbf{0}$. The function $g(\mathbf{x}, \mathbf{Y}) = \mathbf{x}^H \mathbf{Y}^{-1} \mathbf{x}$ is jointly convex in $\mathbf{x}$ and $\mathbf{Y}$ [70]. Let $\mathbf{x} = \mathbf{A}_0 \mathbf{s}$ and $\mathbf{Y} = \mathbf{I} + \sum_{k=1}^{K} q_k \mathbf{A}_k \mathbf{S} \mathbf{A}_k^H$. Both are affine transformations. Thus, $f(\mathbf{s}, \mathbf{S})$ is jointly concave of $\mathbf{s}$ and $\mathbf{S}$.

Since $f(\mathbf{s}, \mathbf{S})$ is jointly concave in $\mathbf{s}$ and $\mathbf{S}$, the first-order approximation of $f(\mathbf{s}, \mathbf{S})$, denoted by $u_1(\mathbf{s}, \mathbf{S}; \mathbf{s}_\ell, \mathbf{S}_\ell)$, is a majorizer of $f(\mathbf{s}, \mathbf{S})$ at the point $(\mathbf{s}_\ell, \mathbf{S}_\ell)$, which is given by

$$
\begin{aligned}
& u_1(\mathbf{s}, \mathbf{S}; \mathbf{s}_\ell, \mathbf{S}_\ell) \\
&= f(\mathbf{s}_\ell, \mathbf{S}_\ell) + \mathcal{D}_{\mathbf{s}} f|_{\mathbf{s}_\ell} (\mathbf{s} - \mathbf{s}_\ell) + \mathcal{D}_{\mathbf{s}^*} f|_{\mathbf{s}_\ell^*} (\mathbf{s}^* - \mathbf{s}_\ell^*) \\
&\quad + \mathrm{Tr}\left(\left(\frac{\partial f}{\partial \mathbf{S}}|_{\mathbf{s}_\ell} \right)^T (\mathbf{S} - \mathbf{S}_\ell) \right) + \mathrm{Tr}\left(\left(\frac{\partial f}{\partial \mathbf{S}^*}|_{\mathbf{s}_\ell^*} \right)^T (\mathbf{S}^* - \mathbf{S}_\ell^*) \right) \\
&= f(\mathbf{s}_\ell, \mathbf{S}_\ell) - \mathbf{s}_\ell^H \left(\mathbf{A}_0^H \left[\Psi(\mathbf{S}_\ell) + \mathbf{I} \right]^{-1} \mathbf{A}_0 \right) (\mathbf{s} - \mathbf{s}_\ell) \\
&\quad - \mathbf{s}_\ell^T \left(\mathbf{A}_0^H \left[\Psi(\mathbf{S}_\ell) + \mathbf{I} \right]^{-1} \mathbf{A}_0 \right)^T (\mathbf{s}^* - \mathbf{s}_\ell^*) \\
&\quad + \mathrm{Tr}\left(\left(\sum_{k=1}^{K} q_k \left(\mathbf{Q}_\ell^k \right)^H \mathbf{S}_\ell \mathbf{Q}_\ell^k \right) (\mathbf{S} - \mathbf{S}_\ell) \right) \\
&\quad + \mathrm{Tr}\left(\left(\sum_{k=1}^{K} q_k \left(\mathbf{Q}_\ell^k \right)^H \mathbf{S}_\ell \mathbf{Q}_\ell^k \right)^T (\mathbf{S}^* - \mathbf{S}_\ell^*) \right) \\
&= -f(\mathbf{s}_\ell, \mathbf{S}_\ell) - 2\mathrm{Re}\left(\left(\mathbf{s}_\ell^H \mathbf{A}_0^H \left[\Psi(\mathbf{S}_\ell) + \mathbf{I} \right]^{-1} \mathbf{A}_0 \right) \mathbf{s} \right) \\
&\quad + 2\mathrm{Tr}\left(\left(\sum_{k=1}^{K} q_k \left(\mathbf{Q}_\ell^k \right)^H \mathbf{S}_\ell \mathbf{Q}_\ell^k \right) \mathbf{S} \right) \\
&\quad - 2\mathrm{Tr}\left(\left(\sum_{k=1}^{K} q_k \left(\mathbf{Q}_\ell^k \right)^H \mathbf{S}_\ell \mathbf{Q}_\ell^k \right) \mathbf{S}_\ell \right). \qquad (61)
\end{aligned}
$$

■

B. Proof of Proposition 4

Proof: Proving $u_{alt}(\mathbf{s}, \mathbf{s}_\ell)$ is a majorizer of $f(\mathbf{s})$ is equivalent to proving that

$$
\begin{aligned}
& \mathbf{s}^H \mathbf{A}_0^H \left[\Psi(\mathbf{s}) + \mathbf{I} \right]^{-1} \mathbf{A}_0 \mathbf{s} \\
& \geq \frac{\mathbf{s}^H \mathbf{A}_0^H \left[\mathbf{\Psi}(\mathbf{s}_\ell) + \mathbf{I} \right]^{-1} \mathbf{A}_0 \mathbf{s}_\ell \mathbf{s}_\ell^H \mathbf{A}_0^H \left[\mathbf{\Psi}(\mathbf{s}_\ell) + \mathbf{I} \right]^{-1} \mathbf{A}_0 \mathbf{s}}{\mathbf{s}_\ell^H \mathbf{A}_0^H \left[\mathbf{\Psi}(\mathbf{s}_\ell) + \mathbf{I} \right]^{-1} \left[\mathbf{\Psi}(\mathbf{s}) + \mathbf{I} \right] \left[\mathbf{\Psi}(\mathbf{s}_\ell) + \mathbf{I} \right]^{-1} \mathbf{A}_0 \mathbf{s}_\ell}, \qquad (62)
\end{aligned}
$$

where the equality is achieved when $\mathbf{s} = \mathbf{s}_\ell$.

Since $[\mathbf{\Psi}(\mathbf{s}) + \mathbf{I}] \succ \mathbf{0}$, a unique positive definite square root, denoted by $\mathit{\Gamma}(\mathbf{s})$, exists. In addition, the denominator of $l_{alt}(\mathbf{s}_\ell, \mathbf{s}_\ell)$ is positive. Then, (62) is equivalent to

$$
\begin{aligned}
& \left\| \mathit{\Gamma}(\mathbf{s})^{-1} \mathbf{A}_0 \mathbf{s} \right\|^2 \left\| \mathit{\Gamma}(\mathbf{s}) \left[\mathbf{\Psi}(\mathbf{s}_\ell) + \mathbf{I} \right]^{-1} \mathbf{A}_0 \mathbf{s}_\ell \right\|^2 \\
& \quad \geq \left| \left\langle \mathbf{A}_0 \mathbf{s}, \left[\mathbf{\Psi}(\mathbf{s}_\ell) + \mathbf{I} \right]^{-1} \mathbf{A}_0 \mathbf{s}_\ell \right\rangle \right|^2. \qquad (63)
\end{aligned}
$$

Due to

$$
\begin{aligned}
& \left| \left\langle \mathbf{A}_0 \mathbf{s}, \left[\mathbf{\Psi}(\mathbf{s}_\ell) + \mathbf{I} \right]^{-1} \mathbf{A}_0 \mathbf{s}_\ell \right\rangle \right| \\
& \quad = \left| \left\langle \mathit{\Gamma}(\mathbf{s})^{-1} \mathbf{A}_0 \mathbf{s}, \mathit{\Gamma}(\mathbf{s}) \left[\mathbf{\Psi}(\mathbf{s}_\ell) + \mathbf{I} \right]^{-1} \mathbf{A}_0 \mathbf{s}_\ell \right\rangle \right|, \qquad (64)
\end{aligned}
$$

we have

$$
\begin{aligned}
& \left\| \mathit{\Gamma}(\mathbf{s})^{-1} \mathbf{A}_0 \mathbf{s} \right\|^2 \left\| \mathit{\Gamma}(\mathbf{s}) \left[\mathbf{\Psi}(\mathbf{s}_\ell) + \mathbf{I} \right]^{-1} \mathbf{A}_0 \mathbf{s}_\ell \right\|^2 \\
& \quad \geq \left| \left\langle \mathit{\Gamma}(\mathbf{s})^{-1} \mathbf{A}_0 \mathbf{s}, \mathit{\Gamma}(\mathbf{s}) \left[\mathbf{\Psi}(\mathbf{s}_\ell) + \mathbf{I} \right]^{-1} \mathbf{A}_0 \mathbf{s}_\ell \right\rangle \right|^2, \qquad (65)
\end{aligned}
$$

which follows the Cauchy-Schwarz inequality with equality holding iff $\mathit{\Gamma}(\mathbf{s})^{-1} \mathbf{A}_0 \mathbf{s} = \mathit{\Gamma}(\mathbf{s}) [\mathbf{\Psi}(\mathbf{s}_\ell) + \mathbf{I}]^{-1} \mathbf{A}_0 \mathbf{s}_\ell$, or equivalently, $\mathbf{s} = \mathbf{s}_\ell$. ■

C. Proof of Proposition 5

Proof: Define $f(\mathbf{x}, \mathbf{Y}) = \frac{\mathbf{x}^H \mathbf{x}}{\mathbf{a}^H \mathbf{Y} \mathbf{a}}$ with $\mathbf{Y} \succ \mathbf{0}$. Let $\mathbf{x} = \mathbf{x}_0 + t\mathbf{x}_1$ and $\mathbf{Y} = \mathbf{Y}_0 + t\mathbf{Y}_1$, with $\mathbf{Y}_0$ being positive definite and $\mathbf{Y}_1$ being symmetric. Since $\frac{d^2 f}{dt^2}|_{t=0} = \frac{2\|\mathbf{x}\|^2}{(\mathbf{a}^H \mathbf{Y}_0 \mathbf{a})^2} \geq 0$, $f(\mathbf{x}, \mathbf{Y})$ is jointly convex in $\mathbf{x}$ and $\mathbf{Y}$. Let $\mathbf{x} = \mathbf{s}_\ell^H \mathbf{A}_0^H [\mathbf{\Psi}(\mathbf{s}_\ell) + \mathbf{I}]^{-1} \mathbf{A}_0 \mathbf{s}$, $\mathbf{a} = [\mathbf{\Psi}(\mathbf{s}_\ell) + \mathbf{I}]^{-1} \mathbf{A}_0 \mathbf{s}_\ell$, and $\mathbf{Y} = \mathbf{I} + \sum_{k=1}^{K} q_k \mathbf{A}_k \mathbf{S} \mathbf{A}_k$. Since $\mathbf{x}$ and $\mathbf{Y}$ are the affine transformation of $\mathbf{s}$ and $\mathbf{S}$, respectively, $u_{alt}(\mathbf{s}, \mathbf{S}; \mathbf{s}_\ell, \mathbf{S}_\ell)$ is jointly concave in $\mathbf{s}$ and $\mathbf{S}$. Thus, the first-order approximation of $u_{alt}(\mathbf{s}, \mathbf{S}; \mathbf{s}_\ell, \mathbf{S}_\ell)$, denoted by

$\widehat{u_{alt}}(\mathbf{s},\mathbf{S};\mathbf{s}_\ell,\mathbf{S}_\ell)$, is a majorizer of $u_{alt}(\mathbf{s},\mathbf{S};\mathbf{s}_\ell,\mathbf{S}_\ell)$ at the point $(\mathbf{s}_\ell,\mathbf{S}_\ell)$, which is given by

$$\begin{aligned}
&\widehat{u_{alt}}\left(\mathbf{s},\mathbf{S};\mathbf{s}_\ell,\mathbf{S}_\ell\right)\\
&= u_{alt}(\mathbf{s}_\ell,\mathbf{S}_\ell;\mathbf{s}_\ell,\mathbf{S}_\ell) + \mathcal{D}_{\mathbf{s}} u_{alt}|\left(\mathbf{s}-\mathbf{s}_\ell\right) + \mathcal{D}_{\mathbf{s}^*} u_{alt}|_{\mathbf{s}_\ell^*}\left(\mathbf{s}^*-\mathbf{s}_\ell^*\right)\\
&+ \mathrm{Tr}\left[\left(\frac{\partial u_{alt}}{\partial \mathbf{S}}|_{\mathbf{s}_\ell}\right)^T\left(\mathbf{S}-\mathbf{S}_\ell\right)\right] + \mathrm{Tr}\left[\left(\frac{\partial u_{alt}}{\partial \mathbf{S}^*}|_{\mathbf{s}_\ell^*}\right)^T\left(\mathbf{S}^*-\mathbf{S}_\ell^*\right)\right]\\
&= \mathbf{s}^H\mathbf{A}_0^H\left[\mathbf{\Psi}\left(\mathbf{S}_\ell\right)+\mathbf{I}\right]^{-1}\mathbf{A}_0\mathbf{s}_\ell\\
&\quad - 2\mathrm{Re}\left(\left(\mathbf{A}_0^H\left[\Psi\left(\mathbf{S}_\ell\right)+\mathbf{I}\right]^{-1}\mathbf{A}_0\mathbf{s}_\ell\right)^H\mathbf{s}\right)\\
&\quad + 2\mathrm{Tr}\left(\left(\sum_{k=1}^{K} q_k\left(\mathbf{Q}_\ell^k\right)^H\mathbf{S}_\ell\mathbf{Q}_\ell^k\right)\mathbf{S}\right)\\
&\quad - 2\mathrm{Tr}\left(\left(\sum_{k=1}^{K} q_k\left(\mathbf{Q}_\ell^k\right)^H\mathbf{S}_\ell\mathbf{Q}_\ell^k\right)\mathbf{S}_\ell\right), \qquad (66)
\end{aligned}$$

which is exactly the same as $u_1(\mathbf{s},\mathbf{S};\mathbf{s}_\ell,\mathbf{S}_\ell)$.

Therefore, $u_1(\mathbf{s},\mathbf{S};\mathbf{s}_\ell,\mathbf{S}_\ell)$ is a majorizer of $u_{alt}(\mathbf{s},\mathbf{S};\mathbf{s}_\ell,\mathbf{S}_\ell)$ with equality holding iff $\mathbf{s}=\mathbf{s}_\ell$. ■

REFERENCES

[1] E. Fishler, A. Haimovich, R. Blum, D. Chizhik, L. Cimini, and R. Valenzuela, "MIMO radar: An idea whose time has come," in *Proc. IEEE Radar Conf.*, Apr. 2014, pp. 71–78.

[2] J. Li and P. Stoica, *MIMO Radar Signal Processing*. New York, NY, USA: Wiley Online Library, 2009.

[3] A. M. Haimovich, R. S. Blum, and L. J. Cimini, "MIMO radar with widely separated antennas," *IEEE Signal Process. Mag.*, vol. 25, no. 1, pp. 116–129, Jan. 2008.

[4] J. Li and P. Stoica, "MIMO radar with colocated antennas," *IEEE Signal Process. Mag.*, vol. 24, no. 5, pp. 106–114, Sep. 2007.

[5] S. A. Vorobyov and M. Lops, "Trade-offs in MIMO radar with colocated antennas," in *Proc. Tuts. 8th IEEE Sensor Array Multichannel Signal Process. Workshop*, A Coruña, Spain, Jun. 2014.

[6] S. Haykin, "Cognitive radar: A way of the future," *IEEE Signal Process. Mag.*, vol. 23, no. 1, pp. 30–40, Jan. 2006.

[7] S. Haykin, Y. Xue, and P. Setoodeh, "Cognitive radar: Step toward bridging the gap between neuroscience and engineering," *Proc. IEEE*, vol. 100, no. 11, pp. 3102–3130, Nov. 2012.

[8] P. Stoica, J. Li, and Y. Xie, "On probing signal design for MIMO radar," *IEEE Trans. Signal Process.*, vol. 55, no. 8, pp. 4151–4161, Aug. 2007.

[9] D. R. Fuhrmann and G. San Antonio, "Transmit beamforming for MIMO radar systems using signal cross-correlation," *IEEE Trans. Aerosp. Electron. Syst.*, vol. 44, no. 1, pp. 171–186, Jan. 2008.

[10] S. Ahmed, J. S. Thompson, Y. R. Petillot, and B. Mulgrew, "Finite alphabet constant-envelope waveform design for MIMO radar," *IEEE Trans. Signal Process.*, vol. 59, no. 11, pp. 5326–5337, Nov. 2011.

[11] A. Aubry, A. D. Maio, and Y. Huang, "MIMO radar beampattern design via PSL/ISL optimization," *IEEE Trans. Signal Process.*, vol. 64, no. 15, pp. 3955–3967, Aug. 2015.

[12] P. Stoica, H. He, and J. Li, "New algorithms for designing unimodular sequences with good correlation properties," *IEEE Trans. Signal Process.*, vol. 57, no. 4, pp. 1415–1425, Apr. 2009.

[13] H. He, P. Stoica, and J. Li, "Waveform design with stopband and correlation constraints for cognitive radar," in *Proc. 2nd Int. Workshop Cogn. Inf. Process.*, Jun. 2010, pp. 344–349.

[14] J. Song, P. Babu, and D. P. Palomar, "Optimization methods for designing sequences with low autocorrelation sidelobes," *IEEE Trans. Signal Process.*, vol. 63, no. 15, pp. 3998–4009, Aug. 2015.

[15] J. Song, P. Babu, and D. Palomar, "Sequence design to minimize the weighted integrated and peak sidelobe levels," *IEEE Trans. Signal Process.*, vol. 63, no. 8, pp. 2051–2064, Apr. 2016.

[16] H. He, P. Stoica, and J. Li, "Designing unimodular sequence sets with good correlations—Including an application to MIMO radar," *IEEE Trans. Signal Process.*, vol. 57, no. 11, pp. 4391–4405, Nov. 2009.

[17] J. Song, P. Babu, and D. P. Palomar, "Sequence set design with good correlation properties via majorization-minimization," *IEEE Trans. Signal Process.*, vol. 64, no. 11, pp. 2866–2879, Jun. 2016.

[18] E. Grossi and M. Lops, "Space-time code design for MIMO detection based on Kullback-Leibler divergence," *IEEE Trans. Inf. Theory*, vol. 58, no. 6, pp. 3989–4004, Jun. 2012.

[19] Y. Yang and R. S. Blum, "MIMO radar waveform design based on mutual information and minimum mean-square error estimation," *IEEE Trans. Aerosp. Electron. Syst.*, vol. 43, no. 1, pp. 330–343, Jan. 2007.

[20] Y. Yang and R. S. Blum, "Minimax robust MIMO radar waveform design," *IEEE J. Sel. Topics Signal Process.*, vol. 1, no. 1, pp. 147–155, Jun. 2007.

[21] A. Aubry, A. De Maio, B. Jiang, and S. Zhang, "Ambiguity function shaping for cognitive radar via complex quartic optimization," *IEEE Trans. Signal Process.*, vol. 61, no. 22, pp. 5603–5619, Nov. 2013.

[22] A. De Maio, S. D. Nicola, Y. Huang, S. Zhang, and A. Farina, "Code design to optimize radar detection performance under accuracy and similarity constraints," *IEEE Trans. Signal Process.*, vol. 56, no. 11, pp. 5618–5629, Nov. 2008.

[23] A. De Maio, S. De Nicola, Y. Huang, Z.-Q. Luo, and S. Zhang, "Design of phase codes for radar performance optimization with a similarity constraint," *IEEE Trans. Signal Process.*, vol. 57, no. 2, pp. 610–621, Feb. 2009.

[24] A. De Maio, S. De Nicola, Y. Huang, D. P. Palomar, S. Zhang, and A. Farina, "Code design for radar STAP via optimization theory," *IEEE Trans. Signal Process.*, vol. 58, no. 2, pp. 679–694, Feb. 2010.

[25] A. De Maio, Y. Huang, and M. Piezzo, "A Doppler robust max-min approach to radar code design," *IEEE Trans. Signal Process.*, vol. 58, no. 9, pp. 4943–4947, Sep. 2010.

[26] A. De Maio, Y. Huang, M. Piezzo, S. Zhang, and A. Farina, "Design of optimized radar codes with a peak to average power ratio constraint," *IEEE Trans. Signal Process.*, vol. 59, no. 6, pp. 2683–2697, Jun. 2011.

[27] A. Aubry, M. Lops, A. M. Tulino, and L. Venturino, "On MIMO detection under non-Gaussian target scattering," *IEEE Trans. Inf. Theory*, vol. 56, no. 11, pp. 5822–5838, Nov. 2010.

[28] E. Grossi, M. Lops, and L. Venturino, "Robust waveform design for MIMO radars," *IEEE Trans. Signal Process.*, vol. 59, no. 7, pp. 3262–3271, Jul. 2011.

[29] E. Grossi, M. Lops, and L. Venturino, "Min-max waveform design for MIMO radars under unknown correlation of the target scattering," *Signal Process.*, vol. 92, no. 6, pp. 1550–1558, 2012.

[30] C.-Y. Chen and P. Vaidyanathan, "MIMO radar waveform optimization with prior information of the extended target and clutter," *IEEE Trans. Signal Process.*, vol. 57, no. 9, pp. 3533–3544, Sep. 2009.

[31] G. Cui, H. Li, and M. Rangaswamy, "MIMO radar waveform design with constant modulus and similarity constraints," *IEEE Trans. Signal Process.*, vol. 62, no. 2, pp. 343–353, Jan. 2014.

[32] P. Setlur and M. Rangaswamy, "Joint filter and waveform design for radar STAP in signal dependent interference," Tech. Rep. AFRL-RY-WP-TP-2015-0170, Oct. 2015.

[33] M. M. Naghsh, M. Soltanalian, P. Stoica, and M. Modarres-Hashemi, "Radar code design for detection of moving targets," *IEEE Trans. Aerosp. Electron. Syst.*, vol. 50, no. 4, pp. 2762–2778, Oct. 2014.

[34] M. M. Naghsh, M. Soltanalian, P. Stoica, M. Modarres-Hashemi, A. De Maio, and A. Aubry, "A Doppler robust design of transmit sequence and receive filter in the presence of signal-dependent interference," *IEEE Trans. Signal Process.*, vol. 62, no. 4, pp. 772–785, Feb. 2014.

[35] A. Aubry, A. De Maio, and M. M. Naghsh, "Optimizing radar waveform and Doppler filter bank via generalized fractional programming," *IEEE J. Sel. Topics Signal Process.*, vol. 9, no. 8, pp. 1387–1399, Dec. 2015.

[36] P. Stoica, H. He, and J. Li, "Optimization of the receive filter and transmit sequence for active sensing," *IEEE Trans. Signal Process.*, vol. 60, no. 4, pp. 1730–1740, Apr. 2012.

[37] A. Aubry, A. DeMaio, A. Farina, and M. Wicks, "Knowledge-aided (potentially cognitive) transmit signal and receive filter design in signal-dependent clutter," *IEEE Trans. Aerosp. Electron. Syst.*, vol. 49, no. 1, pp. 93–117, 2013.

[38] X. Yu, G. Cui, L. Kong, and V. Carotenuto, "Space-time transmit code and receive filter design for colocated MIMO radar," in *Proc. IEEE Radar Conf.*, 2016, pp. 1–6.

[39] Y.-C. Wang, X. Wang, H. Liu, and Z.-Q. Luo, "On the design of constant modulus probing signals for MIMO radar," *IEEE Trans. Signal Process.*, vol. 60, no. 8, pp. 4432–4438, Aug. 2012.

[40] A. Aubry, A. De Maio, M. Piezzo, and A. Farina, "Radar waveform design in a spectrally crowded environment via nonconvex quadratic optimization," *IEEE Trans. Aerosp. Electron. Syst.*, vol. 50, no. 2, pp. 1138–1152, Apr. 2014.
[41] A. Aubry, A. De Maio, M. Piezzo, M. M. Naghsh, M. Soltanalian, and P. Stoica, "Cognitive radar waveform design for spectral coexistence in signal-dependent interference," in *Proc. IEEE Radar Conf.*, May 2014, pp. 0474–0478.
[42] S. Amuru, R. M. Buehrer, R. Tandon, and S. Sodagari, "MIMO radar waveform design to support spectrum sharing," in *Proc. IEEE Military Commun. Conf.*, Nov. 2013, pp. 1535–1540.
[43] P. Stinco, M. S. Greco, and F. Gini, "Spectrum sensing and sharing for cognitive radars," *IET Radar, Sonar Navigat.*, vol. 10, no. 3, pp. 595–602, Mar. 2015.
[44] A. Aubry, V. Carotenuto, A. De Maio, and S. Iommelli, "Cognitive radar waveform design for spectral compatibility," in *proc. IEEE Sensor Signal Process. Defence,* 2016, pp. 1–5.
[45] D. P. Bertsekas, *Nonlinear Programming*. Norwood, MA, USA: Athena Scientific, 1999.
[46] D. R. Hunter and K. Lange, "A tutorial on MM algorithms," *Amer. Statist.*, vol. 58, no. 1, pp. 30–37, 2004.
[47] Y. Sun, P. Babu, and D. P. Palomar, "Majorization-minimization algorithms in signal processing, communications, and machine learning," *IEEE Trans. Signal Process.*, vol. 65, no. 3, pp. 794–816, Feb. 2017.
[48] B. Friedlander, "On signal models for MIMO radar," *IEEE Trans. Aerospace Electron. Syst.*, vol. 48, no. 4, pp. 3655–3660, Oct. 2012.
[49] T. I. Laakso, V. Valimaki, M. Karjalainen, and U. K. Laine, "Splitting the unit delay [FIR/all pass filters design]," *IEEE Signal Process. Mag.*, vol. 13, no. 1, pp. 30–60, Jan. 1996.
[50] J. R. Guerci, *Cognitive Radar: A Knowledge-Aided Fully Adaptive Approach*. Norwood, MA, USA: Artech House, 2010.
[51] G. Cui, X. Yu, V. Carotenuto, and L. Kong, "Space-time transmit code and receive filter design for colocated MIMO radar," *IEEE Trans. Signal Process.*, vol. 65, no. 5, pp. 1116–1129, Mar. 2017.
[52] M. I. Skolnik, *Radar Handbook, 3rd ed*. New York, NY, USA: McGraw-hill, 2010.
[53] J. Capon, "High-resolution frequency-wavenumber spectrum analysis," *Proc. IEEE*, vol. 57, no. 8, pp. 1408–1418, Aug. 1969.
[54] M. Razaviyayn, M. Hong, and Z.-Q. Luo, "A unified convergence analysis of block successive minimization methods for nonsmooth optimization," *SIAM J. Optim.*, vol. 23, no. 2, pp. 1126–1153, 2013.
[55] J.-S. Pang, "Partially B-regular optimization and equilibrium problems," *Math. Oper. Res.*, vol. 32, no. 3, pp. 687–699, 2007.
[56] J.-S. Pang, M. Razaviyayn, and A. Alvarado, "Computing B-stationary points of nonsmooth DC programs," *Math. Oper. Res.*, vol. 42, no. 1, pp. 95–118, 2016.
[57] D. P. Bertsekas *et al.*, *Convex Analysis and Optimization.* Belmont, MA, USA: Athena Scientific, 2003.
[58] J. A. Tropp, I. S. Dhillon, R. W. Heath, and T. Strohmer, "Designing structured tight frames via an alternating projection method," *IEEE Trans. Inf. Theory*, vol. 51, no. 1, pp. 188–209, Jan. 2005.
[59] G. Scutari, D. P. Palomar, and S. Barbarossa, "Cognitive MIMO radio," *IEEE Signal Process. Mag.*, vol. 25, no. 6, pp. 46–59, Nov. 2008.
[60] G. Scutari and D. P. Palomar, "MIMO cognitive radio: A game theoretical approach," *IEEE Trans. Signal Process.*, vol. 58, no. 2, pp. 761–780, Feb. 2010.
[61] Z.-Q. Luo, W.-k. Ma, A. M.-C. So, Y. Ye, and S. Zhang, "Semidefinite relaxation of quadratic optimization problems," *Signal Process. Mag.*, vol. 27, no. 3, p. 20, 2010.
[62] G. Pataki, "On the rank of extreme matrices in semidefinite programs and the multiplicity of optimal eigenvalues," *Math. Oper. Res.*, vol. 23, no. 2, pp. 339–358, 1998.
[63] Y. Huang and D. P. Palomar, "Rank-constrained separable semidefinite programming with applications to optimal beamforming," *IEEE Trans. Signal Process.*, vol. 58, no. 2, pp. 664–678, Feb. 2010.
[64] O. Mehanna, K. Huang, B. Gopalakrishnan, A. Konar, and N. D. Sidiropoulos, "Feasible point pursuit and successive approximation of non-convex QCQPs," *IEEE Signal Process. Lett.*, vol. 22, no. 7, pp. 804–808, Jul. 2015.
[65] M. ApS, *The MOSEK optimization toolbox for MATLAB manual. Version 7.1 (Revision 28)*, 2015. [Online] Available: http://docs.mosek.com/7.1/toolbox/index.html
[66] R. Varadhan and C. Roland, "Simple and globally convergent methods for accelerating the convergence of any EM algorithm," *Scand. J. Statist.*, vol. 35, no. 2, pp. 335–353, 2008.
[67] O. Rabaste, L. Savy, M. Cattenoz, and J.-P. Guyvarch, "Signal waveforms and range/angle coupling in coherent colocated mimo radar," in *Proc. IEEE Radar Int. Conf.*, 2013, pp. 157–162.
[68] G. San Antonio, D. R. Fuhrmann, and F. C. Robey, "MIMO radar ambiguity functions," *IEEE J. Sel. Topics Signal Process.*, vol. 1, no. 1, pp. 167–177, Jun. 2007.
[69] S. M. Karbasi, A. Aubry, A. De Maio, and M. H. Bastani, "Robust transmit code and receive filter design for extended targets in clutter," *IEEE Trans. Signal Process.*, vol. 63, no. 8, pp. 1965–1976, Apr. 2015.
[70] S. Boyd and L. Vandenberghe, *Convex Optimization*. Cambridge, U.K.: Cambridge Univ. Press, 2004.

Linlong Wu received the B.E. degree in electronic information from the Xi' an Jiaotong University, Xi' an, China, in 2014. He is currently working toward the Ph.D. degree in electronic and computer engineering at the Hong Kong University of Science and Technology.

His research interests are in optimization algorithms with applications in signal processing, MIMO radar, and financial engineering.

Prabhu Babu received the Ph.D. degree in electrical engineering from the Uppsala University, Uppsala, Sweden, in 2012.

From 2013 to 2016, he was a Postdoctoral Fellow with the Hong Kong University of Science and Technology. He is currently with the Centre for Applied Research in Electronics, Indian Institute of Technology Delhi, New Delhi, India.

Daniel P. Palomar (S'99–M'03–SM'08–F'12) received the Electrical Engineering and Ph.D. degrees from the Technical University of Catalonia (UPC), Barcelona, Spain, in 1998 and 2003, respectively.

He is a Professor with the Department of Electronic and Computer Engineering, Hong Kong University of Science and Technology (HKUST), Hong Kong, which he joined in 2006. Since 2013, he is a Fellow of the Institute for Advance Study with the HKUST. He had previously held several research appointments, namely, at King's College London, London, U.K.; Stanford University, Stanford, CA, USA; Telecommunications Technological Center of Catalonia, Barcelona, Spain; Royal Institute of Technology, Stockholm, Sweden; University of Rome "La Sapienza," Rome, Italy; and Princeton University, Princeton, NJ, USA. His current research interests include applications of convex optimization theory, game theory, and variational inequality theory to financial systems, big data systems, and communication systems.

Dr. Palomar is the recipient of the 2004/2006 Fulbright Research Fellowship, the 2004 and 2015 (coauthor) Young Author Best Paper Awards by the IEEE Signal Processing Society, the 2015–2016 HKUST Excellence Research Award, the 2002/03 best Ph.D. prize in Information Technologies and UPC, the 2002/2003 Rosina Ribalta first prize for the Best Doctoral Thesis in Information Technologies and Communications by the Epson Foundation, and the 2004 prize for the best Doctoral Thesis in Advanced Mobile Communications by the Vodafone Foundation and COIT. He is a Guest Editor for the IEEE JOURNAL OF SELECTED TOPICS IN SIGNAL PROCESSING 2016 Special Issue on "Financial Signal Processing and Machine Learning for Electronic Trading" and has been an Associate Editor for the IEEE TRANSACTIONS ONINFORMATION THEORYand of IEEE TRANSACTIONS ON SIGNAL PROCESSING, a Guest Editor for the IEEE SIGNAL PROCESSING MAGAZINE2010 Special Issue on "Convex Optimization for Signal Processing," the IEEE JOURNAL ON SELECTED AREAS IN COMMUNICATIONS2008 Special Issue on "Game Theory in Communication Systems," and the IEEE JOURNAL ON SELECTED AREAS IN COMMUNICATIONS 2007 Special Issue on "Optimization of MIMO Transceivers for Realistic Communication Networks."